Title

Loss of ALBINO3b Insertase Results in Truncated Light-Harvesting Antenna in Diatoms1 [OPEN].

Journal

Plant physiology, 181(3)

ISSN

0032-0889

Authors

Nymark, Marianne
Volpe, Charlotte
Hafskjold, Marthe Caroline Grønbech
et al.

Publication Date

2019-11-01

DOI

10.1104/pp.19.00868

Peer reviewed

Plant Physiology Preview. Published on August 30, 2019, as DOI:10.1104/pp.19.00868

SHORT TITLE: Effects of loss of ALB3b insertase in diatoms

CORRESPONDING AUTHOR: Marianne Nymark (marianne.nymark@ntnu.no)

Loss of ALBINO3b insertase results in truncated light-harvesting antenna in diatoms

Marianne Nymark*#[1], Charlotte Volpe*[2], Marthe Caroline Grønbech Hafskjold[1], Henning Kirst[3], Manuel Serif[1], Olav Vadstein[2], Atle Magnar Bones[1], Anastasios Melis[3], Per Winge[1].

*Joint first author

[1]Department of Biology, Norwegian University of Science and Technology, N-7491, Trondheim, Norway

[2]Department of Biotechnology and Food Science, Norwegian University of Science and Technology, N-7491, Trondheim, Norway

[3]Department of Plant and Microbial Biology, UC Berkeley, Berkeley, California 94720, USA

ONE SENTENCE SUMMARY:

Diatom ALB3b is required for insertion of Fx-Chl binding proteins in thylakoid membranes and has a novel conserved domain implying that its interaction partners differ from those in plants/green algae.

AUTHOR CONTRIBUTIONS:

M.N., A.M.B., O.V., A.M., and P.W. conceived the research plans. M.N., A.M.B., A.M., and P.W. supervised and designed the experiments. M.N., C.V., M.C.G.H., H.K., and M.S. performed the experiments. M.N., C.V., M.C.G.H., H.K, A.M., and P.W. analyzed the data. M.N. and C.V. wrote the article with contributions of all the authors. M.N. agrees to serve as the author responsible for contact and ensures communication.

FUNDING:

This work was supported by a grant from the Research Council of Norway to A.M.B through funding of the project "Downsizing light-harvesting antenna to scale up production potential and valorization from cultivation of marine microalgae" (project no. 267474), a Peder Sather Grant Award to A.M. and A.M.B. (Peder Sather Foundation Grant Number: SRPSC4 1-50504-13618-44 ME1AM), the NTNU enabling technologies program to P.W., and a grant from the Research Council of Norway to O.V. through funding of the project Microbially Produced Raw Materials for Aquafeed (MIRA; project no. 239001).

ABSTRACT

The family of chloroplast ALBINO3 (ALB3) proteins function in the insertion and assembly of thylakoid membrane protein complexes. Loss of ALB3b in the marine diatom *Phaeodactylum tricornutum* leads to a striking change of cell color from the normal brown to green. A 75% decrease of the main fucoxanthin-chlorophyll *a/c*-binding proteins was identified in the *alb3b* strains as the cause of changes in the spectral properties of the mutant cells. The *alb3b* lines exhibit a truncated light-harvesting antenna phenotype with reduced amounts of light-harvesting pigments and require a higher light intensity for saturation of photosynthesis. Accumulation of photoprotective pigments and LHCX proteins were not negatively affected in the mutant strains, but still the capacity for non-photochemical quenching was lower compared to wild type. In plants and green algae, ALB3 proteins interact with members of the chloroplast signal recognition particle pathway through a lysine-rich C-terminal domain. A novel conserved C-terminal domain was identified in diatoms and other stramenopiles, questioning if ALB3b proteins have the same interaction partners as their plant/green algae homologs.

INTRODUCTION

Diatoms (*Bacillariophyceae*) are a major group of eukaryotic phytoplankton belonging to the phylum Heterokont that evolved through a secondary endosymbiotic event around 200 to 180

million years ago (Brown and Sorhannus, 2010). Diatoms are key primary producers in the marine food chain. They account for 40% of the total carbon fixation in oceans and 25% of the total global oxygen production (Falkowski et al., 1998). Diatom plastids differ substantially from the ones in green algae and land plants due to their peculiar inheritance and evolution (Oudot-Le Secq et al., 2007). Because of secondary endosymbiotic events, four membranes surround the diatom chloroplast. The outer envelope, known as chloroplast endoplasmic reticulum, is a continuum with the nuclear envelope. The diatom thylakoids are organized in stacked bands of three membranes, also known as girdle lamellae, spanning along the entire length of the plastid. This configuration differs substantially from the classic grana stacks and interconnecting stroma-exposed thylakoid organization found in higher plant chloroplasts (Austin and Staehelin, 2011). Light-harvesting complexes (LHCs) are embedded in the thylakoid membrane of the chloroplast and surround the photosynthetic reaction centers of the photosystems.

In contrast to land plants, where specific LHCs serve either PSI or PSII, diatoms are characterized by a peripheral fucoxanthin (Fx)-chlorophyll (Chl) *a/c* antenna complex believed to deliver excitation energy to both photosystems, in addition to having a PSI-associated antenna (Lepetit et al., 2010; Büchel, 2015). Proteins of the peripheral Fx-Chl *a/c* antenna complex in diatoms belong to the LHC superfamily (Durnford et al., 1996), but are often referred to as Fx-Chl *a/c* binding proteins (FCPs) in order to distinguish them from the LHCs of the green lineages (Falkowski and Raven, 2007). In addition to the light-harvesting pigments, FCPs also bind diadinoxanthin (Ddx) and diatoxanthin (Dtx), photoprotective pigments essential during light stress conditions (Wang et al., 2019). The FCPs belong to three major LHC classes: the LHCF, including the main Fx-Chl *a/c* binding proteins, the red algal-like LHCRs, and the LHCXs, related to the LhcSRs in *Chlamydomonas reinhardtii* (Büchel, 2015). The latter has been shown to play a central role in dissipating excessively absorbed energy through non-photochemical quenching (NPQ) in cooperation with photoprotective pigments (Bailleul et al., 2010; Taddei et al., 2016; Lepetit et al., 2017; Taddei et al., 2018).

LHC proteins and certain photosystem core proteins are known to be integrated into the thylakoid membrane of land plants and green microalgae through the post-translational or co-translational part of the chloroplast signal recognition particle (CpSRP) assembly pathway (Sundberg et al.,

1997; Schuenemann et al., 1998; Bellafiore et al., 2002; Gerdes et al., 2006; Kirst et al., 2012; Kirst et al., 2012; Kirst and Melis, 2014). The plant/green algae CpSRP pathway includes the LHC specific chaperon CpSRP43, the GTPase CpSRP54, the signal recognition receptor CpFTSY, and the ALBINO3 insertase (ALB3) (Bellafiore et al., 2002; Kirst and Melis, 2014). Homologs of CpSRP54, CpFTSY, and ALB3 can be identified in diatom genomes (Armbrust et al., 2004; Bowler et al., 2008; Mock et al., 2017), whereas no homolog for the molecular chaperon CpSRP43 have been identified (Träger et al., 2012). CpSRP43 orthologs appear to be restricted to plants and green algae, however distantly related ankyrin repeat proteins can be found in Haptophyceae. Diatom CpSRP54 knockout mutants have been shown to be light sensitive (Nymark et al., 2016), but no further information exists about CpSRP54's role, or the role of any other members of the CpSRP pathway, in integration and assembly of thylakoid membrane proteins in diatoms. It has been shown, however, that efficient integration of FCPs depend on stromal factors and on the presence of GTP (Lang and Kroth, 2001).

In land plants and green microalgae, members of the CpSRP pathway guide certain chloroplast proteins to the thylakoid membranes where ALB3 mediates protein insertion in the developing thylakoids. ALB3 belongs to the YidC/Oxa1/Alb3 family of proteins that function in folding, insertion, and assembly of membrane protein complexes in bacteria and in certain eukaryotic organelles, such as mitochondria and chloroplasts (Hennon et al., 2015). The homologs within each subfamily have different C-terminal domains that are crucial for their function and protein-protein interaction. Two homologs belonging to this protein family are found in the chloroplasts of *Arabidopsis thaliana*, ALB3 and ALB4 (Sundberg et al., 1997; Gerdes et al., 2006) and *C. reinhardtii*, ALB3.1 and ALB3.2 (Bellafiore et al., 2002). ALB3 mutants of *A. thaliana* have a severe phenotype. They are characterized by white/pale-yellow leaves, are defective in thylakoid membrane development, have strongly decreased pigment content and are unable to survive phototrophically beyond the seedling stage when grown on soil (Sundberg et al., 1997). The *A. thaliana* ALB3 insertase is essential for insertion of LHC proteins through the post-translational CpSRP pathway and seems to be involved in co-translational assembly of certain chloroplast-encoded membrane proteins (Sundberg et al., 1997; Moore et al., 2000; Kugelmann et al., 2013). Functional data exist also for the two *C. reinhardtii* ALB3 homologs, ALB3.1 and ALB3.2 (Bellafiore et al., 2002; Ossenbühl et al., 2004; Göhre et al., 2006). The ALB3.1 of *C. reinhardtii*

has been shown to be crucial for insertion of LHC proteins into the developing thylakoid membrane and to play a role in the assembly of D1 reaction center protein into PSII (Bellafiore et al., 2002; Ossenbühl et al., 2004). In contrast to the *A. thaliana* ALB3 mutants, *C. reinhardtii* cells lacking ALB3.1 are still capable of phototrophic growth. The other *C. reinhardtii* ALB3 homolog, ALB3.2, is however essential for cell survival and is believed to be associated with the assembly and maintenance of the photosystems (Göhre et al., 2006).

Important differences have been identified between the function of the ALB3 homologs of organisms within the green lineage. We therefore hypothesized that characterization of diatom ALB3 insertases have the potential to uncover other and unique functional features connected to this protein family. Using a reverse genetics approach, we applied the CRISPR/Cas9 technology to knock out *ALB3b*, encoding one of the two ALB3 proteins present in the diatom *Phaeodactylum tricornutum*. We demonstrate here that ALB3b's primary functional role pertains to insertion of light-harvesting antenna proteins in the developing thylakoid membrane. This, however, does not include antenna proteins functioning in photoprotection. Reduced levels of light-harvesting antenna proteins resulted in changes in the spectral properties, pigment content, growth rate, and photosynthetic performance of the cells.

RESULTS

Two homologs of the ALB3 insertase were identified in *P. tricornutum* and in all other stramenopiles where sequence data are available (Supplemental Figure S1). Phylogenetic analyses showed that ALB3 proteins in plants/green algae and ALB3 proteins from stramenopiles were clearly divided into two distinct groups (Supplemental Figure S1). Sequence similarity with the two ALB3 proteins with known functions in the green algae *C. reinhardtii* could therefore not be used to predict the individual function of the two *P. tricornutum* ALB3 proteins (ALB3a and ALB3b). The ALB3a paralog has a basic lysine-rich C-terminal domain (CTD) with similarities to CTD domains in ALB3 proteins in plants and green algae (Supplemental Figure S2). In *A. thaliana* this domain has been reported to interact directly with CpSRP43 and CpSRP54·CpFTSY complexes (Falk et al., 2010; Falk and Sinning, 2010; Lewis et al., 2010; Dünschede et al., 2011;

Chandrasekar and Shan, 2017). ALB3b proteins in stramenopiles, however, do not contain the lysine-rich CTD but have instead a unique conserved domain (Figure 1). Both *P. tricornutum* *ALB3* genes (*ALB3a* (Phatr2_43657) and *ALB3b* (Phatr2_46411)) were targeted for CRISPR/Cas9-mediated disruption, but we were only able to generate viable knockout (KO) lines for the *ALB3b* gene. Three independent *alb3b* KO lines (*alb3b-14*, *alb3b-16*, *alb3b-19*) with large insertions of different sizes toward the 5' end of the gene (Supplemental Figure S3) were identified and cultured from single cells. All insertions consisted of fragments of the vectors used for transformation and caused premature stop codons at the N-terminal part of the protein (Figure 1B). To verify that both alleles were mutated and that no wild-type (WT) sequence was present, allele-specific PCR was performed. Both alleles could be amplified in the WT whereas only one allele could be amplified in the mutant strains, indicating larger insertion or deletion events which prevent amplification of the other mutated allele by PCR (Supplemental Figure S4). Complementation of all three *alb3b* KO mutants with a codon modified *ALB3b* (to avoid gene editing) was performed to confirm that the phenotype described below was the result of a lack of a functional ALB3B insertase.

Spectral properties of WT and *alb3b* mutants

Previous studies on green algae and plants showed that mutations causing a reduction in the size of the light-harvesting antenna result in a pale green color of the chloroplasts (Sundberg et al., 1997; Bellafiore et al., 2002; Polle et al., 2003; Kirst et al., 2012; Kirst et al., 2012; Oey et al., 2013; Gu et al., 2017). The diatom FCP complexes contain, in addition to Chl *a* and *c*, high amounts of Fx responsible for the golden-brown coloration of the diatom cells (Gundermann and Büchel, 2014; Büchel, 2015; Wang et al., 2019). The absorption properties of Fx are strongly dependent on the protein environment, and undergo extreme bathochromic shifts upon protein binding, dividing the different Fx molecules into more red, green, and blue absorbing complexes (Premvardhan et al., 2009; Premvardhan et al., 2010; Gundermann and Büchel, 2014; Wang et al., 2019). We therefore hypothesized that a distortion of the normal antenna size/structure of *P. tricornutum* could result in a visible change in cell coloration. Disruption of the gene encoding the ALB3B insertase did indeed cause a change in coloration from the normal golden brown of the WT cells, to a green coloration, suggesting structural changes of the light-harvesting antenna

176 in the *alb3b* KO mutants (Figure 2A).
177
178 To further explore the visual changes in spectral properties in the *alb3b* mutants compared to WT
179 cultures, we recorded the *in vivo* absorbance (Figure 2B) and fluorescence excitation spectra
180 (Figure 2C) for medium light (ML) acclimated cultures. The spectra showed that less light energy
181 in the blue-green region is absorbed and available for photosynthesis in cultures lacking the
182 ALB3b insertase. *In vivo* fluorescence excitation spectra were used to indicate the pigments'
183 relative energy transfer efficiency (ETE) to Chl *a* in the reaction center of PSII (RCII). The
184 differences in the *in vivo* fluorescence excitation spectra between WT and *alb3b* mutants (Figure 2C**,**
185 inset) strongly resembled the absorption characteristics of Chl *c* (peak at 462 nm) and Fx (peak at 520
186 nm) (Bricaud et al., 2004; Premvardhan et al., 2009; Gundermann and Büchel, 2014), implying a
187 substantially lower contribution in energy transfer from Chl *c* and Fx to RCII in the *alb3b* KO mutants.
188 Smaller differences between WT and mutant strains are expected for the absorption spectra, as these
189 spectra will also include pigments associated with PSI and non-protein bound carotenoids dissolved
190 in the thylakoid membrane that do not transfer absorbed energy to PSII (Lepetit et al., 2010). Even so,
191 the difference in the peak profile for the absorption spectra (Figure 2B, inset) matches the difference
192 in the *in vivo* fluorescence excitation spectra confirming a reduction of Chl *c* and Fx in the mutants.
193
194 Low temperature (77 K) fluorescence measurements were performed to clarify the distribution of
195 excitation energy between PSII and PSI in WT compared to *alb3b* mutant cultures (Figure 3). The
196 same samples were excited with either 435 nm (targeting Chl *a* absorption maxima; Figure 3A) or 470
197 nm (targeting antenna pigments (Chl *c* and carotenoids; Figure 3B)). 77 K emission spectra recorded
198 from ML acclimated samples revealed fluorescence emission maxima at 688 nm and 710 nm, which
199 are traditionally attributed to PSII and PSI, respectively (Ikeda et al., 2008; Yamagishi et al., 2010;
200 Juhas and Buchel, 2012). In addition, an increase in fluorescence at 710 nm (F_{710}) emission at the
201 expense of F_{687} was observed in *P. tricornutum* cells that were in a state of high NPQ (Lavaud and
202 Lepetit, 2013). In WT samples the chosen excitation wavelengths caused a preferential energy transfer
203 to PSII, displaying a relative amplitude of PSII fluorescence emission that was 2.5-fold (435 nm) or
204 3.3-fold (470 nm) higher than the PSI emission (F_{687}/F_{710}). In contrast, the average F_{687}/F_{710} observed
205 in the *alb3b* mutants were F_{687}/F_{710}= 1.3 (435 nm) or 1.4 (470 nm), implying that excitation energy
206 transfer to PSII was relatively more affected than energy transfer to PSI.

Effect of lack of ALB3b insertase on the organization of photochemical apparatus

The green color of the *alb3b* KO mutants and the combined results from the absorbance, fluorescence excitation, and emission spectra suggested that these mutants have an altered functional light-harvesting antenna size. To investigate this in more detail, the WT and the *alb3b* KO lines were analyzed using an absorbance difference spectrophotometer (Melis, 1989). The rate of light absorption per second by PSII and PSI was measured by using low intensity actinic light selected by cut-off and interference filters to selectively excite Fx (533 nm) or Chl *a* (670 nm), respectively (Table 1). When exiting Fx, the rate of light utilization by the photosystems revealed a severe decrease in the absorption cross-section both for PSII and for PSI in the *alb3b* mutant lines compared to WT (Table 1). The functional Chl *a* antenna size of PSII and PSI in the mutants were less affected because of the Chl *a* molecules bound to the photosystem core subunits (Ben-Shem et al., 2003; Nelson and Yocum, 2006; Ago et al., 2016) (Table 1). In accordance with the 77 K data, these data also suggest a more severe decrease of the antenna size of the PSII compared to the PSI (Table 1).

Organization of the photochemical apparatus was further studied by quantification of PSI (P700) relative to the Chl *a* content of the cells. P700 content was measured from the light induced ΔA_{700} absorbance change at 700 nm attributed to photooxidation of P700. On a P700 basis, there was a substantially lower number of Chl *a* molecules in the *alb3b*, i.e., from 663 Chl *a*/P700 in the WT, down to an average of 425 Chl *a*/P700 in the mutants (Table 1). This directly reflects the lowering of Chl *a* pigments per electron transport chain (i.e., per P700) in the *alb3b* mutants relative to the WT.

Western blot was used for examination of the role of the ALB3b insertase in incorporating proteins in the thylakoid membrane. Antibodies specific for antenna proteins (LHCFs and LHCXs) and photosystem subunits (D1, D2, and PsaC) were used, and an antibody against AtpB was employed as a loading control. The level of LHCF proteins in the *alb3b* mutants was assessed by an antibody binding to a highly conserved epitope of the LHCF1 to LHCF11 proteins (Juhas et al., 2014), and found to be lowered to about 25% of WT levels in cells grown under both LL and ML conditions (Figure 4A). The relative decline of LHCF proteins is in good agreement with the smaller

functional antenna size of PSII, as estimated from the kinetic spectrophotometric measurements using Fx excitation (Table 1). The relative gene expression levels of four *LHCF* genes (*LHCF1*, *LHCF2*, *LHCF5*, and *LHCF8*) were examined to determine if the low content of LHCF proteins in the *alb3b* lines could be explained by a strong downregulation of the expression of these genes. Our data showed high gene expression levels (low Ct-values) of the examined *LHCF*s in all lines (Supplemental Table S1). Of the examined LHCF genes, only *LHCF8* was significantly, but moderately, down-regulated in all *alb3b* lines (Supplemental Figure S5). No antibodies are available for detection of LHCR proteins constituting the main LHC protein fraction associated the PSI antenna (Lepetit et al., 2010; Grouneva et al., 2011; Gundermann and Büchel, 2014). However, the smaller functional PSI antenna size in the mutant lines implied that ALB3b plays a vital role also in insertion of LHCR proteins. An antibody (anti-FCP6) against an LHCX (FCP6) of *Cyclotella meneghiniana*, which also cross-react with the *P. tricornutum* LHCX proteins (Juhas et al., 2014), was used for comparison of the relative content of these photoprotective proteins. LHCX1 is crucial for NPQ to take place, whereas LHCX2-3 can provide additional NPQ capacity during high light stress (Bailleul et al., 2010; Taddei et al., 2016; Lepetit et al., 2017; Taddei et al., 2018). LHCX1 and LHCX3 are of highly similar size (21.9 kDa and 22.8 kDa, respectively), therefore complete separation by western blot analysis is challenging. Based on the expression pattern of the LHCX isoforms known from literature, we interpret the proteins detected under both LL and ML conditions to be a mix of LHCX1 and LHCX3 with the major contribution coming from LHCX1 under these conditions (Taddei et al., 2016; Taddei et al., 2018). The relative content of the LHCX1+3 proteins in the mutants compared to WT seemed to be unaffected (slightly reduced levels of LHCX1+3 in *alb3b-14*) in both light conditions (Figure 4A). The LHCX2 protein (24.7 kDa) was detected at similar levels in WT and *alb3b* lines after 6 h of ML exposure (Supplemental Figure S6B), but it was not detectable in LL- or ML-acclimated samples (Figure 4A). The strong band of ~22 kDa detected in WT and *alb3b* lines 6 h after the shift from LL to ML (Supplemental Figure S6B) is likely to contain large amounts of LHCX3 in addition to LHCX1 (Taddei et al., 2016; Taddei et al., 2018). Based on Western blot analyses performed on PSI/II core proteins, the lack of a functional ALB3b insertase does not seem to have a negative impact on the incorporation of chloroplast-encoded photosystem subunits (Figure 4B).

Preliminary analysis with transmission electron microscopy (TEM) showed a lower number of thylakoid membranes per chloroplast, but no obvious difference in the thylakoid architecture could

be observed in the *alb3b-14* mutant line acclimated to LL (Supplemental Figure S7).

Functional properties of the *alb3b* KO mutants

To study the capability of the *alb3b* mutant to respond to a shift in light conditions, LL-acclimated cells (0 h) were shifted to ML conditions and sampled after 0.5, 6, 24, 48, and 168 h. The pigment content (Figure 5) and photosynthetic performance (Figures 6 and 7) of the acclimating cells were analyzed.

Capacity for photoacclimation and photoprotection

As expected from the changed coloration and spectroscopic analyses, the *alb3b* KO mutants had a significantly lower content of light-harvesting pigments (LHPs) per cell compared to WT (Figure 5). Even though the content of LHPs in LL-acclimated *alb3b* mutants was already lower than in ML-acclimated WT cells, the LHP concentration in the mutants decreased further as a response to the ML treatment (Figure 5A-B). This observation implies that the mechanisms controlling the downregulation of the LHPs in response to an increase in available light are independent of the actual pigment concentration in the cells. The *alb3b* mutant lines contained ~40-60 % less Chl *a* and ~60-65 % less Fx in response to the light treatment (Figure 5A-B, Supplemental Table S2).

The smaller antenna size of the mutant lines had no negative impact on the cell content of the xanthophyll cycle carotenoids Ddx and Dtx (Figure 5C-D). Both WT and *alb3b* mutant lines showed the expected photoprotective response to a shift to a higher light intensity (Nymark et al., 2009), which could be observed as an immediate rise in Dtx concentration inversely to a decrease in Ddx concentration. The conversion of Ddx to Dtx peaked at the 0.5 h time point as evident by the de-epoxidation state (DES) index (Figure 6A). The DES index decreased and stabilized at a lower level after prolonged exposure to ML, indicating that the algae were acclimating to the new light condition. Although changes in DES index for both WT and mutants followed the same pattern after the shift to higher light intensities, the DES index were higher in the mutants than in WT cultures at all time points. The NPQ capacity of the *alb3b* mutants was initially (approx. two months after isolation of mutated single cells) found to be lowered to around half of that in the WT

297 levels at irradiance levels > 400 μmol m^{-2} s^{-1} (Figure 6B), but when the same experiment was
298 repeated after the cells had been maintained in culture for one more year (approx. 100-150
299 generations) the differences between WT and mutants had declined for all lines (Figure 6C).
300 Measurements of time-dependent NPQ development in *alb3b* mutants and WT produced highly
301 similar results as when calculating NPQ from rapid light curves (Supplemental Figure S8). The
302 NPQ of *alb3b-16* was closer to WT levels whereas a lower NPQ was observed in the two other
303 *alb3b* lines. The smaller differences in NPQ capacity between *alb3b* lines and WT led us to also
304 re-analyze the relative LHCF protein content, pigment levels, and photosynthetic parameters in
305 LL-acclimated *alb3b* and WT cultures after one more year of growth (Supplemental Figures S6A,
306 S9-S10). No major changes were observed for the *alb3b* lines relative to WT cells compared to
307 the initial analyses of these parameters.

308

309 **Photosynthetic performance**

310 Variable Chl *a* fluorescence (Pulse-Amplitude-Modulation (PAM) fluorescence measurements)
311 was used to calculate the photosynthetic (PSII) efficiency (F_v/F_m,) of WT and mutant lines during
312 the light experiment. In LL-acclimated cells, the F_v/F_m were ~0.7 for all lines (Figure 7A), which
313 is around the maximum value expected for algal cells under optimal growth conditions (Falkowski
314 and Raven, 2007). After 0.5 h of ML exposure, both WT and mutant cells showed a modest
315 decrease in F_v/F_m (Figure 7A). The F_v/F_m in the mutant cultures stabilized close to ~0.6 in ML,
316 whereas F_v/F_m in WT cultures increased after prolonged exposure to ML. The maximum relative
317 electron transport rate ($rETR_{max}$) and light saturation index (E_k) values increased as a function of
318 ML exposure time in all cultures (Figure 7C-D), as the photoacclimation mechanisms enabled the
319 cells to utilize the increased amount of light energy available for photosynthesis (Nymark et al.,
320 2009). However, the *alb3b* mutants displayed, on average, a ~30-40% higher $rETR_{max}$ and E_k
321 compared to WT cultures, showing the largest differences during the first part of the light
322 experiment before the cells had been able to downsize the photosynthetic apparatus in response to
323 the increased light intensities. Less pronounced differences in $rETR_{max}$ and E_k were found between
324 WT and *alb3b* cultures at the 24 h time point due to a more rapid change in photoacclimation status
325 in WT cells, probably because of a higher cell division rate as described below (Table 3). To further
326 investigate the apparent increased photosynthetic performance of the *alb3b* KO lines indicated by

the PAM measurement, light-saturation curves of photosynthesis (P-E curves) based on oxygen evolution, were measured for WT and *alb3b* KO lines acclimated to either LL (Figure 7E) or ML (Figure 7F). The maximum photosynthetic rate (P_{max} (µmol O_2/ mol Chl/s), the maximum light utilization coefficient (α), and the saturation intensity (E_s) of photosynthesis (P_{max}/α (µmol photons m^{-2} s^{-1})) were calculated from the P-E curves (Table 2) (Powles and Critchley, 1980). When normalized to Chl *a*, the mutant lines showed a typical truncated light-harvesting antenna (TLA) - mutant phenotype with higher P_{max} and E_s and slightly lower α compared to WT due to lower functional absorption cross-section caused by the smaller antenna (Kirst et al., 2014). Thus, it should be noted that these results do not indicate a higher photosynthetic performance per cell. In fact, when oxygen evolution was normalized per cell, the mutant lines showed a P_{max} similar to WT (Supplemental Figure S11). Also, the light saturation curves of the *alb3b* KO lines acclimated to LL showed a tendency of declining photosynthetic activity at light intensity > 1000 µmol photons m^{-2} s^{-1} (Figure 7E).

Effect of light intensity on cell growth

Growth parameters were calculated from the exponential phase in batch cultures of LL- and ML-acclimated cultures (Table 3; Supplemental Figure S12) to investigate how the changes in antenna size and composition affected the cell division rate. The results showed that WT cells grew faster than *alb3b* KO mutants at both light conditions, but a shift from LL to ML intensities diminished that growth rate gap between the *alb3b* KO mutants and WT (Table 3), as recently observed in other TLA mutants (Kirst et al., 2014; Formighieri and Melis, 2017). At ML conditions the WT cells already divided at a maximum rate slightly above two cell divisions per day (Fawley, 1984). We hypothesized that if the slower growth rate of the *alb3b* mutants were caused by a lower ability to capture light energy, increasing the light intensities should have a positive effect on growth of the mutant cells. To investigate if a further increase in light intensity could close the growth rate gap, mutants and WT cells were acclimated to high light conditions (HL; 480 µmol photons m^{-2} s^{-1}). The growth temperature was set to 23°C which supports the highest cell division rate in *P. tricornutum* (Fawley, 1984). During the HL acclimation period (two weeks), the majority of the cells in one of the *alb3b* lines (*alb3b-16*) changed from the fusiform morphotype to a rounded phenotype. The rounded cells showed a tendency for aggregation, making accurate counting

necessary for growth rate calculations difficult. The attempt to acclimate *alb3b-16* to HL was repeated after the discovery of the strongly increased NPQ capacity in cells that had been maintained in culture for one year after isolation of single cells, but the HL treatment induced the same change in morphotype as previously observed. The two other *alb3b* lines did not show a change in morphotype during the HL acclimation period or during the following growth rate experiments, but prolonged HL treatment (months) including periods in stationary phase, induced the formation of the rounded cell type also in the two other *alb3b* lines. The same treatment did not provoke the formation of round cells in WT cultures. Growth curves are included in Supplemental Figure S13A. The growth rate calculations from the exponential part of the curve, showed that the WT cells still divided twice per day in HL, whereas the average maximal growth rate of the *alb3b* mutants dropped from 1.2 in ML to 0.8 divisions per day under HL (Table 3). The physiological status of the cells, measured as F_v/F_m, was monitored during the length of the growth experiment (Supplemental Figure S13B). The average F_v/F_m in WT cultures during the period of maximal growth, was found to be 0.63. In contrast, the corresponding F_v/F_m value in the *alb3b* mutants were 0.41, pointing to a higher degree of photodamage. In order to investigate presence of oxidative damage, levels of lipid peroxidation were measured for HL-acclimated WT and mutant cells (*alb3b-14*, *alb3b-19*). The mutant lines did not show higher levels of lipid peroxidation compared to the WT (Supplemental Figure S14). Similar levels of xanthophyll pigments in the mutant compared to the WT could explain these results, considering their role in the stabilization and protection of the thylakoid membrane lipids from peroxidation (Hauvaux et al., 2007).

Complementation studies of *alb3b* mutants

A plasmid containing the codon modified *ALB3b* under control of its native promoter was introduced to the three *alb3b* lines by biolistic bombardment. As a result, 70 of in total 75 transformed colonies regained their brown coloration. Six brown colonies (two colonies derived from each of the three complemented lines) were randomly picked and subjected to PCR analysis followed by sequencing. The introduction of the modified *ALB3b* gene and the absence of WT sequence were confirmed (Supplemental Figure S15). Three brown colonies (representing each of the three complemented mutant lines) were cultured for analyses of pigment and LHCF content. The results showed that the WT phenotype was recovered by introduction of the modified *ALB3b*

387 gene (Figure 8).

DISCUSSION

Effects of loss of the *P. tricornutum* ALB3b insertase

The substantially lower level of antenna proteins belonging to the LHCF group (Figure 4A) indicate that the primary role of the *P. tricornutum* ALB3b insertase is the efficient integration of the main LHC proteins into the thylakoid membrane. However, a small functional antenna size is still assembled, implying a phenotype where some LHC proteins can be inserted through other thylakoid membrane insertion pathways, or that some functional redundancy exists between ALB3b and the uncharacterized diatom homolog ALB3a. The mainly unaffected levels of photoprotective LHCX proteins found in *alb3b* mutants (Figure 4A) clearly indicate the presence of other integration pathway(s) for antenna proteins. The lower level of LHPs and smaller functional antenna size, the changed spectral properties, and the increased light saturation level, can be seen as effects of the lower amount of antenna proteins causing a truncated light-harvesting antenna. The phenotypic traits listed above are characteristic of TLA-phenotype mutants, previously generated in cyanobacteria, green microalgae, and land plants (Polle et al., 2003; Kirst et al., 2012; Kirst et al., 2012; Kirst et al., 2014; Formighieri and Melis, 2017; Gu et al., 2017; Kirst et al., 2017; Kirst et al., 2018). TLA mutants have been shown to grow at relatively similar rates as WT when enough light energy is available (Bellafiore et al., 2002; Polle et al., 2003; Kirst et al., 2014; Gu et al., 2017).

The slow growth of the *alb3b* mutants compared to WT cells might be partially explained by a reduced ability to capture light energy, since an increase in light intensity from 35 (LL) to 200 µmol photons m^{-2} s^{-1} (ML) diminished the difference in growth rate between WT and mutant by a factor of 2. If the smaller antenna size of the mutants were the sole reason for the slow growth rate, a further increase in irradiance should further diminish the difference in growth between WT and mutant. Instead, analyses of algae cultures acclimated to HL (~480 µmol photons m^{-2} s^{-1}) revealed a negative effect on cell division rate, photodamage of the *alb3b* mutants, and induction of a round cell phenotype. The round or oval cell shape has previously been reported to be associated with prolonged exposure to abiotic stress (De Martino et al., 2007; De Martino et al., 2011; Herbstova et al., 2017). The apparent increased photosynthetic capacity estimated for *alb3b* mutants at both LL and ML light conditions seems counter intuitive if the *alb3b* mutants are high light sensitive. However, these data are calculated from light-response curves where the algae are subjected to high light intensities for

418 relative short periods of time (minutes). The high light experienced by the algae during the generation
419 of light-response curves might be too short for extensive photodamage to occur. However, mutants
420 acclimated to LL conditions did show signs of photoinhibition observed as a decrease in oxygen
421 production when exposed to light intensities > 1000 µmol photons m^{-2} s^{-1} (Figure 7E).

422

423 NPQ is an important photoprotective mechanism providing the ability to dissipate excessively
424 absorbed energy harmlessly as heat during high light exposure. In the *alb3b* mutants the NPQ capacity
425 was reduced compared to WT levels (Figure 6B-C and Supplemental Figure S7), suggesting a reduced
426 capability to handle prolonged high light exposure. Several studies show a convincing relationship
427 between the amount of both LHCX and Dtx and the capacity for NPQ, and the presence of LHCX
428 proteins and the conversion of protein bound Ddx to Dtx has been found to be essential for NPQ to
429 take place (Lavaud et al., 2002; Bailleul et al., 2010; Lepetit et al., 2012; Lepetit et al., 2013; Lepetit
430 et al., 2017; Taddei et al., 2018). The level of LHCX proteins and the content of the xanthophyll cycle
431 pigments (Ddx+Dtx) were not negatively affected by the lack of ALB3b insertase. However, Ddx
432 and Dtx are found in three different pools in diatoms, one located in a lipid shield around the FCPs,
433 and two that are bound to antenna proteins connected to PSI or the peripheral FCP antenna,
434 respectively (Lepetit et al., 2010). Only the protein bound fraction of the peripheral antenna
435 contributes to NPQ after conversion of Ddx to Dtx (Lepetit et al., 2010). Because of the potential to
436 store xanthophyll cycle pigments in the lipid phase of the thylakoid membrane, the amount of
437 accumulated Ddx+Dtx that are protein bound might still be reduced even though the cell
438 concentrations in the *alb3b* lines are similar or higher than in WT. The molecular role of LHCX and
439 Dtx in NPQ is still elusive, and no data exists about the precise localization of FCPs or the LHCX
440 proteins. The latest models for NPQ in diatoms suggest that there are two quenching sites (Q1 and
441 Q2) present in the diatom thylakoids (Miloslavina et al., 2009; Büchel, 2014; Lavaud and Goss, 2014;
442 Goss and Lepetit, 2015; Giovagnetti and Ruban, 2017). NPQ at Q1 is believed to involve physical
443 detachment of FCP oligomers from PSII that in *P. tricornutum* can be measured as an increase in 77
444 K emission at 710 nm and as a decrease of PSII cross-section (Lavaud and Lepetit, 2013; Giovagnetti
445 and Ruban, 2017), whereas Q2 seems to take place in FCPs functionally connected to PSII, and
446 involve antenna reorganization and aggregation of LHC trimers (Miloslavina et al., 2009; Büchel,
447 2014; Lavaud and Goss, 2014; Giovagnetti and Ruban, 2017). Q2 is suggested to be dependent on
448 the presence of protein bound Dtx and provides a much higher level of NPQ compared to Q1

(Giovagnetti and Ruban, 2017). Despite the comparable content of photoprotective antenna proteins and pigments in WT and *alb3b* mutants, the strong decrease in *alb3b* antenna size might disturb crucial protein-pigment or protein-protein (e.g LHCF-LHCX) interactions potentially necessary for effective antenna aggregation (Q2) and lower the pool of detachable antenna involved in Q1. This might lead to the lower NPQ capacity observed in the *alb3b* mutants. However, the difference in NPQ capacity between *alb3b* lines and WT decreased after the *alb3b* lines had been maintained in culture for one additional year (approx. 100-150 generations). The increase in NPQ compared to WT was especially prominent for *alb3b-16*. No major differences in pigment or LHCF content between the individual *alb3b* lines or changes in the pigment or LHCF ratios between *alb3b* and WT were observed that could explain the changes in NPQ capacity over time. The different NPQ levels in the mutants and the general increase in NPQ over time in the *alb3b* lines compared to WT levels can therefore not be explained by changes in antenna size over time. Giovagnetti and Ruban (Giovagnetti and Ruban, 2017) showed that the amount of antenna detached are not proportional to the level of NPQ, and that the NPQ can continue to increase without a further reduction of the PSII cross-section. We therefore suggest that the increase in NPQ over time is caused not by a larger pool of detachable antenna, but that the *alb3b* lines, over many generations, have been able to increase their capacity for NPQ at Q2 through an unknown mechanism.

Role of diatom ALB3b in integration of nucleus and plastid encoded proteins compared to ALB3 in green algae and plants

P. tricornutum ALB3b showed functional similarities with the *C. reinhardtii* homolog ALB3.1 (Bellafiore et al., 2002; Ossenbühl et al., 2004). Both the diatom ALB3b and the green algae ALB3.1 play a role in insertion of LHC proteins into the thylakoid membrane (Bellafiore et al., 2002; Kirst and Melis, 2014), and loss of the insertase causes a notably smaller antenna size (Bellafiore et al., 2002). In addition, *C. reinhardtii* cells lacking ALB3.1 contain a substantially increased fraction of highly stable membrane inserted, but unassembled D1 protein (Ossenbühl et al., 2004). The D1 content in *C. reinhardtii alb3.1* mutants was half of that of WT cells. Based on the above described findings, an additional role in assembly of D1 into PSII was identified in green microalgae (Bellafiore et al., 2002; Ossenbühl et al., 2004). Subunits of PSI (PsaC), PSII (D1, D2), and ATP synthase complex (AtpB) were not negatively affected by the absence of the ALB3b insertase in diatom cells (Figure 4B), but our analyses does not discriminate between unassembled proteins in the thylakoid

membrane and proteins that are incorporated into photosynthetic complexes. More extensive protein analyses would be necessary to rule out a role of the diatom ALB3b insertase in integration/assembly of chloroplast-encoded thylakoid membrane proteins. Assembled PSII complexes are fully functional in both *C. reinhardtii* (Ossenbühl et al., 2004) and *P. tricornutum alb3b* mutants (Figure 7A). We detected no differences in photosynthetic efficiency in LL-acclimated cells between WT and mutants. This implies that even though the *alb3b* KO lines have a truncated antenna size, there is no difference in the probability of the trapped excitation energy being used for photochemistry between WT and mutants. However, a less efficient repair of PSII from photodamage (Guenther and Melis, 1990) and an associated slower replacement of damaged D1 could explain the on average ~12-14% lower F_v/F_m measured in *alb3b* mutants during prolonged ML exposure, and the on average ~36% lower F_v/F_m observed in HL-acclimated mutant cells. An efficient PSII repair mechanism including a more frequent replacement of photodamaged D1 is required under such conditions (Baroli and Melis, 1996; Theis and Schroda, 2016). Alternatively (or additionally), the PSII of the *alb3b* mutants might be more susceptible to photodamage because of the altered light-harvesting antenna disturbing the normally efficient NPQ mechanism (Figure 6B-C) functioning in this alga (Lavaud and Goss, 2014). However, the transformation of the normally fusiform *alb3b-16* line into the rounded morphotype in HL regardless of having a lower (Figure 6B) or more similar (Figure 6C and Supplemental Figure S7) NPQ capacity as WT indicates that there are other reasons for why *alb3b* mutants are sensitive to HL.

The *A. thaliana alb3p* mutant has also been reported to be photosensitive. The mutant requires very low light intensities (12 µmol photons m^{-2} s^{-1}) to produce detectable levels of photosynthetic complexes like LHC trimers and PSII monomers and dimers (Kugelmann et al., 2013). To explain the severe phenotype of the *alb3p* mutants, additional functions beyond the CpSRP pathway have been suggested for ALB3p (Kugelmann et al., 2013). Based on phenotypic similarities between *alb3p* and mutants defective in carotenoid synthesis, it has been speculated that ALB3p has a role in integration and assembly of carotenoids into photosynthetic complexes (Kugelmann et al., 2013). The slow growth of the *P. tricornutum alb3b* mutants that cannot be compensated by increased light intensities, and the susceptibility to prolonged high light exposure, suggest additional roles for the ALB3b insertase. A future comparison with other types of *P. tricornutum* TLA mutants will be valuable for dissecting primary effects of the absence of ALB3b from the secondary effects of having a truncated light-harvesting antenna size.

CONCLUSION

Our results show that ALB3b is essential for assembly of a full-size light-harvesting antenna in diatoms. In land plants and green algae, ALB3 insertases are part of the CpSRP pathway and the basic lysine-rich CTD is necessary for the interaction with other members of the pathway (Bellafiore et al., 2002; Chandrasekar and Shan, 2017). We also identified this domain within the ALB3a proteins of the stramenopiles, but not in the ALB3b proteins which have a unique CTD domain. The LHC-specific chaperone CpSRP43 is one of ALB3's known interaction partners through its lysine-rich CTD domain, but neither we nor others (Träger et al., 2012) could identify this chaperone in diatoms or other stramenopiles. Also, the *P. tricornutum* CpSRP54 mutant was not reported to have a changed coloration, only to be light sensitive (Nymark et al., 2016). The different CTD domain in ALB3b proteins, the absence of CpSRP43, and the unchanged coloration of the diatom CpSRP54 mutant, imply that the ALB3b proteins have distinct interaction partners than those of ALB3a and ALB3 of plants and green algae. A hypothetical model for the role of diatom ALB3 insertases is presented in Figure 9. For verification of the model, a more thorough investigation of the *P. tricornutum* CpSRP54 mutant, and characterization of diatom FTSY mutants should be performed. This will clarify if ALB3b is part of the post-translational CpSRP pathway, or if diatom LHC proteins are guided to ALB3b through other mechanisms.

MATERIALS AND METHODS

An axenic *Phaeodactylum tricornutum* culture originating from the sequenced clone Pt1 8.6 (CCMP2561) was obtained from the culture collection of the Provasoli-Guillard National Center for Marine Algae and Microbiota (NCMA), Bigelow Laboratory for Ocean Sciences.

Experimental conditions

Axenic culturing of *P. tricornutum* WT cells and the three *alb3b* KO lines (*alb3b-14*, *alb3b-16*, and *alb3b-19*) were performed as described previously unless otherwise stated (Nymark et al., 2009). Cell cultures were grown at 15°C under continuous cool white fluorescent light at scalar irradiance (E_{PAR}) of ~35 µmol photons m^{-2} s^{-1} (LL), or ~200 µmol photons m^{-2} s^{-1} (ML). For the high light (HL)

541 experiment the WT and the three independent *alb3b* KO lines were acclimated to 480 µmol m^{-2} s^{-1} and grown at 23°C in a Vötsch VB 1514 plant growth chamber (Vötsch Industrietechnik GmbH, Germany) equipped with metal halide lamps (Powerstar HQI-BT 400 W/D). The cultures were kept in the exponential growth phase for at least three weeks under these conditions to ensure that all cells were fully acclimated prior to conducting measurements.

For the spectrophotometric and kinetic analysis, cells were grown in F/2 enriched artificial seawater media (Guillard and Ryther, 1962). To avoid carbon limitation during growth the media were supplemented with $NaHCO_3$ (final concentration of 23.5 mM, pH=7.4). Cultures were grown at 25 °C in 2 L glass bottles constantly stirred to ensure homogenous growth. Continuous illumination was provided by white fluorescent LED light tubes at ML. For the measurements, 80-85% of the total culture volume was harvested during the mid-exponential growth phase.

Growth rates

Growth rates were estimated in batch cultures of WT and *alb3b* KO lines (three biological replicates) acclimated to LL, ML, or HL using a starting concentration of 100,000 (ML, HL) or 200,000 (LL) cells/ml. Counting was performed either manually using a Bürker-Türk counting chamber after fixation with Lugol`s solution (LL samples) or with a BD Accuri C6 Flow Cytometer (BD Bioscience; ML and HL samples). For the latter, glutaraldehyde (2% v/v final solution) was used for fixation of cells. Samples were excited by a 20 mW 488 nm Solid State Blue laser and chlorophyll fluorescence was measured by a >670 nm optical filter (FL3). The average maximum growth rates (cell division/day) were calculated by using a mean of the growth rates from the three biological replicates during the exponential phase.

Phylogenetic analyses

ALBINO3 proteins in the NCBI (National Center for Biotechnology Information) protein database and from the iMicrobe transcriptome database (https://www.imicrobe.us/) were selected for phylogenetic analyses. Accession numbers for the protein sequences used in the analysis are listed in Supplemental Table S4. The analysis involved 47 ALB3 proteins from plants and algae, each species was represented with two ALB3 paralogs (ALB3.1/ALB3.2 or ALB3a/ALB3b). The protein alignment was generated by using the ClustalX program (Thompson et al., 1997) and manually

refined in GeneDoc 2.7.000 (Nicholas et al., 1997). The evolutionary relationships were estimated using the maximum likelihood (ML) method based on the Le-Gascuel model (Le and Gascuel, 2008) and the neighbor-joining method (Saitou and Nei, 1987). The initial trees for both ML and NJ analyses were obtained automatically by applying Neighbor-Join and BioNJ algorithms to a matrix of pairwise distances, estimated using a JTT model and the trees with best topology were selected. For the ML-analyses, a discrete Gamma distribution was used to model evolutionary rate differences among sites (using 5 categories). All positions with less than 80% site coverage were eliminated. Tree branch confidence values were calculated by running 1000 bootstrap replicates for NJ and 100 replicates for ML. The phylogenetic analyses were conducted in MEGA7 (Kumar et al., 2016).

CRISPR/Cas9 gene editing of the ALB3b insertase

All steps for performing CRISPR/Cas9 editing of the *ALB3b* insertase gene (Phatr2_46411; XM_002180751) including selection of target site, ligation of adapter for target of interest into the pKS diaCas9-sgRNA plasmid (Nymark et al., 2016), transformation of diatom cells, and screening and identification of cells with biallelic mutations, were performed as described in the published protocol for CRISPR/Cas9 gene editing in *P. tricornutum* (Nymark et al., 2017). *ALB3b* specific oligos for creation of the adapter inserted into the sgRNA cassette of the CRISPR/Cas9 vector, and primers used for screening of cells with CRISPR/Cas9-mediated mutations, are presented in Supplemental Table S5. Three *alb3b* KO lines named *alb3b-14*, *alb3b-16*. and *alb3b-19* were selected for functional characterization. These three selected lines were checked for off-target mutations by PCR amplification and sequencing of the regions containing the five most likely off-target sites. To identify potential off-target sites, a custom-made Perl-based script was used to search the genome for sites with high homology to seed (PAM-proximal) region of the target site. The script uses a string-based approach, which allows for up to 3 mismatches in the seed region. Off-targets are ranked by their similarity to the target site as well as the position of the mismatches. No off-target mutations were found at any of the investigated sites. The Phatr2 ID for the genes containing the potential off-target sites and primers used for the screening process are listed in Supplemental Table S5.

Allele-specific PCR

Allele-specific PCR was performed as an additional control as previously described (Serif et al., 2017). In short, primers for PCR were derived which include an allele-specific difference on the 3′

603 terminal base (see primers in Supplemental Table S5), thereby preventing polymerases without
604 proofreading function from amplifying the respective other allele. Both alleles were amplified
605 separately using HiDi polymerase (myPols, Konstanz, Germany) according to the manufacturer's
606 instructions.

607

608 **Isolation of thylakoid membranes**

609 Cells were harvested by centrifugation at 1000 g for 8 min at 4 °C. The pelleted cells were
610 resuspended in 50 mM Tricine – NaOH (pH 7.8) in ice-cold isolation buffer containing 300 mM
611 sucrose, 5 mM $MgCl_2$, 10 mM NaCl, 2% PVP (w/v), 0.1% BSA (w/v), and 5 mM ascorbic acid. The
612 pellet was washed twice with the described buffer to remove residual salts from the growth media.
613 Cells were broken using a Branson 250 sonicator (pulse mode, 50% duty cycle, output power of 5)
614 with a precooled tip for 45 s followed by 1 min of cooling in dim light. This process was repeated
615 four times to ensure rupture of the majority of the cells. Unbroken cells were removed by
616 centrifugation at 6500 rpm for 10 min at 4 °C. The thylakoid suspension was centrifuged at 75,000 g
617 for 45 min at 4°C using a Beckman Coulter ultracentrifuge. The thylakoid pellet was resuspended in
618 5 ml of ice-cold Tricine-NaOH (pH 7.8) buffer containing 10 mM NaCl and 5 mM $MgCl_2$. Samples
619 were measured immediately upon preparation.

620

621 **Spectrophotometric and kinetics analysis**

622 Photosystem kinetics and PSI quantitation analysis were performed using a laboratory-constructed
623 absorbance difference spectrophotometer (Melis and Brown, 1980; Melis, 1989). The premise for
624 this method is that, under light limiting conditions, the rate of primary photochemistry is directly
625 proportional to the light-harvesting antenna size (Melis, 1989). PSI (P_{700}) content was measured from
626 the light-induced ΔA_{700} using a differential extinction coefficient of 64 mM^{-1} cm^{-1} (Hiyama and Ke,
627 1972). Actinic excitation was provided in the red region of the spectrum using a transmittance
628 interference 670 nm filter combined with a yellow cut-off filter (CS 3-69). The reaction mixture
629 contained 50-100 µM Chl *a*, 0.02% SDS (w/v), 250 µM methyl viologen (MV), and 2.5 mM Na-
630 ascorbate. The sample was illumined once prior to measuring to ensure oxidation of Cytochrome c_6
631 and possibly of Cytochrome *f*. Two or three experimental replicates were measured, with at least
632 three technical replicates taken. Chl *a* concentration in the samples was calculated after extraction in

90% acetone (v/v) for 30 min in the dark using the Jeffrey-Humphrey equation for diatoms (Jeffrey and Humphrey, 1975). Photocatalytic kinetics of the two photosystems were measured based on Chl *a* fluorescence induction for PSII and P_{700} oxidation for PSI (Melis, 1989). Actinic illumination was provided in the red and green regions of the spectrum using narrow interference filters with transmittance peaks at 670 nm and a 533 nm. These filters were chosen after examination of the thylakoid absorbance spectra so that the 670 nm filter would excite predominantly Chl *a,* whereas the 533 nm filter would excite Fx and other carotenoids. Incident light intensity provided was 12 μmol photons m^{-2} s^{-1} in the green and 2.1 μmol m^{-2} s^{-1} in the red region. The reaction mixture for the fluorescence kinetic measurements contained approximately 5-10 μM Chl *a* and 20 μM 3-(3,4-dichlorophenyl)-1,1-dimethylurea (DCMU), and that for the P700 oxidation kinetics contained 100-200 μM Chl *a*, 250 μM MV, and 20 μM DCMU.

Absorbance spectra

To avoid light scattering, absorption spectra were measured from thylakoid membrane extracts. Prior to measurement, the samples were placed in darkness in an ice bath to avoid thermal breakdown of thylakoid structure. Absorbance spectra of all extracts were scanned spectrophotometrically from 400 to 750 nm with a Shimadzu UV-1800 UV−visible spectrophotometer. The resuspension buffer was used as a blank and for baseline calibration.

***In vivo* fluorescence excitation**

In vivo fluorescence excitation spectra (400-700 nm) were measured as described previously using a Hitachi F-3000 spectrofluorometer (Nymark et al., 2013). Spectra were obtained by recording the Chl *a* fluorescence intensity (Chl *a* fluorescence from PSII) at 1 nm spectral resolution (5 nm bandwidth) at a fixed wavelength of emission (730 nm, 5 nm bandwidth). The emission of light was measured as a function of absorbed light at different wavelengths for ML-acclimated cultures. All spectra were normalized to the red emission maximum of Chl *a* of the WT cultures, so as to study the differences in excitation energy transfer efficiency (ETE) by the main photosynthetic pigments Chl *a*, Chl *c*, and Fx in the blue-green part of the PAR spectrum, where they exhibit their maximum absorption.

663 **77 K chlorophyll fluorescence emission measurements**

664 Low-temperature fluorescence emission spectra were recorded for three biological replicates of ML-
665 acclimated cell cultures using a custom-made 77 K fluorometer (Lamb et al., 2015). Monochromatic
666 LEDs with an emission centered around either 435 nm (LED435-12-30, Roithner LaserTechnikor) or
667 470 nm (LED470 Roithner LaserTechnikor) were used as excitation wavelengths. Fluorescence
668 emission spectra were recorded between 600 and 800 nm. Samples were adjusted to a Chl
669 concentration of 1 µg/mL, transferred to glass tubes, and frozen in liquid nitrogen before measuring
670 the 77 K fluorescence emission. All spectra were normalized to the WT emission spectrum at 710
671 nm.
672
673 **Protein isolation, SDS-PAGE, and Western blot analysis**

674 WT and *alb3b* mutant cultures acclimated to either LL or ML (three biological replicates for each
675 line and light condition) were harvested by filtration (Durapore Membrane Filters, pore size 0.65
676 µm; Merck Millipore). Filters were transferred to 2 ml tubes (Sarstedt) and 1 ml F/2 medium was
677 added. The tubes were vortexed for 10 s for resuspension of the cells, before removal of filters and
678 centrifugation of re-suspended cells at 16,000 *g* for 1 min at 15 °C. The supernatant was removed
679 and the remaining pellet was flash frozen in liquid nitrogen and stored at -80 °C. A 5 mm pre-cooled
680 stainless-steel bead (QIAGEN) was added to each of the tubes with frozen cell pellets, and the cells
681 were mechanically broken and homogenized in two steps using the TissueLyser system (QIAGEN).
682 The samples were first placed in a precooled (-80 °C) adapter set followed by cell disruption for 2
683 min at 25 Hz. Before the second shaking step (8 min at 25 Hz), the samples were transferred to a
684 room temperature (RT) adapter set and 700 µl lysis buffer (50 mM Tris, pH 6.8, 2% (w/v) SDS)
685 were added according to Juhas et al. (Juhas et al., 2014). Insoluble material was removed by
686 centrifugation (100 *g* for 30 min at 4 °C). The supernatant was transferred to new tubes and the
687 protein concentration was determined using the DC Protein Assay kit (BioRad) following the
688 manufacturer's instructions. In addition to the whole cell extracts, lysates were also obtained from
689 thylakoids isolated from cell cultures acclimated to either LL or ML conditions. Thylakoids were
690 resuspended in lysis buffer (50 mM Tris, pH 6.8, 2% (w/v) SDS) and protein extracts were obtained
691 as above (the first step for cell breakage was omitted). Proteins were resolved on 12% or 15% SDS–
692 PAGE gels, depending of the size of the protein of interest. 10 µg of the protein extracts were
693 loaded onto the gel lanes. Western blot analyses were performed on either total protein extracts

694 (detection of LHCF and LHCX proteins) or thylakoid extracts (detection of D1, D2, and PsaC
695 proteins). The PsaC antibodies produced a signal only when using thylakoid extracts, whereas the
696 antibody recognizing LHCX proteins produced optimal results when using whole cell extracts. LHC
697 proteins and photosystem subunits were therefore analyzed in different extracts. The signal generated
698 by AtpB polyclonal antibodies was used as loading controls on each blot, in addition to Coomassie
699 stained gels that were run in parallel. 10 µg of the protein extracts were loaded onto the gels.
700 Proteins were detected with the following antibodies: anti-D1 (AS05 084 Agrisera; 1:20000), anti-
701 D2 (AS06 146 Agrisera; 1:5000), anti-PsaC (AS10 939 Agrisera; 1:1000), anti-AtpB (AS05 085,
702 Agrisera; 1:4000), anti-LHCF1-11 (1:1000), and anti-FCP6 (LHCX; 1:1000) (kind gifts from C.
703 Büchel, University of Frankfurt, Germany (Juhas et al., 2014)). Primary antibody incubation was
704 performed overnight at 4°C for all antibodies. Polyclonal Goat Anti-Rabbit
705 Immunoglobulins/Biotinylated (Dako) was used as secondary antibody with an incubation time of 2
706 h at RT, followed by incubation with Horseradish Peroxidase Streptavidin (Vector Laboratories) for
707 1 h at RT. Protein-antibody cross-reactions were visualized with SuperSignal West Pico PLUS
708 Chemiluminescent Substrate (Thermo Scientific) and documented with a G:BOX ChemiXRQ gel
709 doc system (Syngene).
710
711 **Transmission electron microscopy**
712 Electron microscopy was used to examine the status of the thylakoid architecture in the *alb3b* mutant
713 lines. WT and *alb3b-14* cell cultures acclimated to LL were harvested by a light centrifugation step
714 (4000 g for 10 min) and fixed overnight at RT in a F/2 medium buffer containing 2.5% glutaraldehyde
715 (v/v) and 2% paraformaldehyde (v/v). Pellets were washed three times in F/2 medium buffer solution
716 and embedded in a 5% (w/v) gelatin solution. After post-fixation in 2% osmiumtetraoxide (w/v) and
717 1.5% kaliumferrocyanid (w/v), the samples were dehydrated in a gradient of ethanol. Samples were
718 thereafter embedded with epoxy resins based on Bozzola and Russell's protocol (Bozzola and Russell,
719 1999) and sectioned with an ultramicrotome. Images were taken using a Tecnai 12 transmission electron
720 microscope operating at 80 kV. Images were captured using a MORADA CCD camera.
721
722 **Measurements of malondialdehyde content**
723 The malondialdehyde (MDA) content was determined using the Lipid Peroxidation (MDA) assay kit
724 (Sigma-Aldrich). The MDA concentration was measured based on its reaction with thiobarbituric
725 acid (TBA) and used as an index of lipid peroxidation. WT and *alb3b (alb3b-14, alb3b-19)* mutant

cultures (three biological replicates for each line) acclimated to HL were harvested by filtration as described above. The cell pellet was resuspended in the MDA lysis buffer. To ensure complete lysis the cells were briefly sonicated. Thereafter, the MDA content was determined based on the manufacturer's instructions. In parallel samples were collected and manually counted to determine cell concentration.

Isolation of total RNA and reverse transcription quantitative PCR

Three biological replicates of LL-acclimated WT and *alb3b* mutant cultures were harvested for isolation of total RNA in parallel to the samples harvested for protein analyses as described above. Total RNA isolation, quantification, and verification of RNA integrity were performed as described in Nymark et al. (Nymark et al., 2009). Reverse transcription of RNA was performed with the QuantiTect Reverse Transcrition kit (Qiagen) following the recommended protocol. 1 µg of total RNA was used in each reaction. Reverse transcription quantitative PCR (RT-qPCR) analysis was performed as described in Nymark et al. (Nymark et al., 2009) for calculation of relative expression ratios of four *LHCF* genes (*LHCF1*, *LHCF2*, *LHCF5*, and *LHCF8*). The geNorm module in the qBasePLUS software (Biogazelle) was used for determining the expression stability of the candidate reference gene. Based on the stability analysis, *RPS5* (Phatr2_42848) and *DLST* (Phatr2_45557) were selected as reference genes (Nymark et al., 2013; Valle et al., 2014). LinRegPCR software (Ramakers et al., 2003; Ruijter et al., 2009) was used to calculate mean PCR efficiency per amplicon and cycle threshold (Ct) values per sample. These data were imported into the qBasePLUS software (Biogazelle), which calculated relative expression ratios (given as Calibrated Normalized Relative Quantities (CNRQ)) and performed statistical analyses on the results. The one-way ANOVA test integrated in the qBasePLUS software was used to evaluate the significance of the estimated relative expression ratios. Forward and reverse primers are listed in Supplemental Table S5.

Light shift time-series experiments

LL-acclimated WT and *alb3b* KO lines were transferred to ML conditions and sampled after 0.5, 6, 24, 48, and 168 h following the shift in growth light intensity. LL samples (0 h) were harvested as controls. Three biological replicates were set up for each line and time point to reach a cell concentration of maximum 1 x 10^6 cells/ml at the day of harvesting. Samples were harvested for pigment analyses, monitoring of cell concentrations, variable *in vivo* Chl *a* fluorescence (PAM), and

protein analyses.

Pigment analyses

HPLC pigment analysis was performed according to Rodriguez et al. (Rodriguez et al., 2006) using a Hewlett-Packard HPLC 1100 Series system. Pigment values from the HPLC analysis were calculated as fmol pigment per cell. Cell numbers were calculated from flow cytometer counts as described above.

Measurements of photosynthetic parameters

A PhytoPAM (System I, Walz, Germany) was used to measure variable Chl *a* fluorescence of the harvested samples. The photosynthesis *vs.* irradiance relationship was obtained as described previously (Nymark et al., 2009). An additional step at 1216 µmol photons m^{-2} s^{-1} was added for the samples that had been treated with ML for 1 week to ensure that light saturation levels were reached. The maximum quantum yield of PSII (F_v/F_m), the maximum relative electron transport rate ($rETR_{max}$), the maximum light utilization coefficient (α), and the light saturation index (E_k) were calculated as described before (Nymark et al., 2009). The $rETR_{max}$ is an estimate of the maximum photosynthetic capacity of the cells (~P_{max}), whereas the light saturation index E_k ($rETR_{max}/\alpha$) is a proxy for the threshold irradiance that separates light-limited and light-saturated photosynthesis (Genty et al., 1989; Sakshaug et al., 1997). F_m at low light intensities is commonly observed to be lower than the F_m' level under low actinic light in diatoms (Serôdio et al., 2006; Cruz and Serôdio, 2008; Cruz et al., 2011). NPQ was therefore calculated from the light-response curve from LL-acclimated samples, using the maximum F_m' level ($F_m'_{max}$;) instead of F_m as follows: $NPQ = (F_m'_{max}/ F_m') - 1$ (Serôdio et al., 2006; Kalaji et al., 2017). NPQ development over time was additionally calculated from LL-acclimated cells exposed to 5 min of actinic light at an intensity setting of 832 µmol photons m^{-2} s^{-1}. For the HL experiment, F_v/F_m was measured with an AquaPen-C (Photon System Instruments) at the end of a 30 min dark acclimation period to relax the fast-reversible component (qE) of NPQ so that only the photoinihibitory, slowly reversible quenching (qI), caused by damaged PSII reaction centers, would influence the F_v/F_m value.

Oxygen evolution was measured at 15 °C using a S1 Clark Type polarographic oxygen electrode (Hansatech) increasingly illuminated with a 35 W cool white spot LED. The measurements were done

on cultures acclimated to both LL and ML. 2 ml cell suspension from mid-exponential phase culture was added to a stirred chamber with temperature control and supplemented with sodium bicarbonate (30 µl of a 0.5 M solution) so that the oxygen production would not be limited by carbon availability. Prior to measuring, the Chl *a* concentration in the sample was adjusted to a concentration lower than 1.2 µM to avoid cell shading in the chamber. Simultaneously, cell concentration of the samples was determined by flow cytometry counting. Oxygen consumption in darkness was measured as a starting baseline, thereafter the sample was exposed to gradually increasing light intensities and the oxygen evolution was measured continuously for at least 10 min. Each light intensity was adjusted by measuring the light intensity in the middle of the electrode chamber with a spherical US-SQS sensor (Waltz).

Complementation of *alb3b* KO lines

A modified version of the *ALB3b* gene was synthesized together with its native promoter by GeneArt® Services Thermo Fisher Scientific Inc (Supplemental Figure S16). Modifications consisted of changes of the codon usage in the PAM and target region of the *ALB3b* gene to avoid gene editing by the functional CRISPR/Cas9 system incorporated into the genome of the *alb3b* KO lines. *Mss*I sites were included at the 5' and 3' ends of the module to facilitate blunt-end cloning into the pM9_4Compln vector from Madhuri et al. (Madhuri et al., 2019) containing the *bsr* gene conferring resistance to blasticidin-S. Transformation of all three *alb3b* KO lines with the pM9_4Compln vector containing the synthesized *ALB3b* module was performed as described previously (Nymark et al., 2017). The algae were transferred to low-salt selection plates (25% (v/v) natural seawater supplemented with f/2-Si, 1% (w/v) agar, 4 µg/mL blasticidin-S (Thermo Fisher Scientific)) ~ 24 h after transformation. Transformed colonies appeared 3-4 weeks after transfer to selection plates. Colonies that had regained the normal brown color were randomly picked from the selection plates. PCR amplification of the *ALB3b* gene and subsequent sequencing were used to test for the presence of the modified version of the *ALB3b* gene and the absence of WT sequence. Primers used for both PCR amplification and sequencing were PtAlb3b-G1F and PtAlb3b-G1R (Supplemental Table S5). One complemented *alb3b* colony, resulting from each of the transformations performed with the *alb3b* KO lines, was cultivated for pigment and protein analyses, as described above.

Statistical analyses

The one-way ANOVA test integrated in the qBasePLUS software (Biogazelle) was used to evaluate the significance of the estimated relative expression ratios of LHCF genes in *alb3b* mutants compared to WT cells. Two-tailed Student t-tests were used to assess if there were significant differences in pigment concentration and photosynthetic parameters between *alb3b* mutants and WT.

ACCESSION NUMBERS:

Accession numbers for ALBINO protein sequences extracted from GenBank NCBI, the iMicrobe database (Marine Microbial Eukaryote Transcriptome Sequencing Project (MMETSP)) and from the JGI genome portal are listed in Supplemental Table S4.

SUPPLEMENTAL DATA:

Supplemental Figure S1: Phylogenetic relationship between members of the ALBINO3 family.

Supplemental Figure S2: C-terminal domain of diatom ALB3a and ALB3b proteins.

Supplemental Figure S3: DNA sequences for the *ALB3b* WT gene and the inserts in the *alb3b* KO lines.

Supplemental Figure S4: Allele-specific amplification of the Cas9 target site within the *ALB3b* gene in WT and *alb3b* mutant strains.

Supplemental Figure S5. Relative expression levels of LHCF genes in *alb3b* lines compared to WT.

Supplemental Figure S6. Western blot analysis of LHCF and LHCX proteins from WT and *alb3b* mutant lines.

Supplemental Figure S7. Transmission electron micrographs of WT and *alb3b-14* mutant line cells.

Supplemental Figure S8. NPQ development over time in WT and *alb3b* lines.

Supplemental Figure S9. Re-evaluation of pigment concentrations per cell for LL-acclimated WT and *alb3b* mutant lines. **Supplemental Figure S10.** Re-evaluation of photo-physiological responses of LL-acclimated WT and *alb3b* mutant lines.

Supplemental Figure S11. Light-saturation curves of photosynthesis for LL- and ML-acclimated WT and *alb3b* mutant lines presented as oxygen evolution per cell.

Supplemental Figure S12: Growth curves for WT and *alb3b* mutants.

Supplemental Figure S13: Growth curves and corresponding measurements of photosynthetic efficiency of WT and *alb3b* mutants in high light.

Supplemental Figure S14: Malondialdehyde (MDA) product of lipid peroxidation.

Supplemental Figure S15: PCR analysis and Sanger sequencing of PCR products from complemented *alb3b* lines.

Supplemental Figure S16: DNA sequence representing the synthetic *ALB3b* module used for complementation of the *alb3b* KO lines.

Supplemental Table S1: Cycle threshold (Ct) values for LHCF and reference genes

Supplemental Table S2: Fraction of Chl *a* and Fx content in *alb3b* mutant lines compared to WT in LL (0h) and after 0.5-168 h in ML.

Supplemental Table S3: Oxygen evolution values of the light-saturation curves of photosynthesis including ±SD for LL- and ML-acclimated WT and *alb3b* mutant lines.

Supplemental Table S4: Accession numbers for ALBINO proteins included in the phylogenetic analyses.

Supplemental Table S5: Oligo and primer sequences.

ACKNOWLEDGEMENTS:

We wish to thank Professor Claudia Büchel for kindly providing LHCF and LHCX antibodies and Professor Peter Kroth for the pM9_4Compln vector. The authors would also like to thank Kjersti Andresen for assistance with the HPLC analyses, Professor Geir Johnsen and Inga Aamot for access to and guidance on use of the PhytoPAM, and Associate professor Martin F. Hohmann-Marriot and Gunvor Røkke for training on how to produce and analyze 77 K data. The authors would like to thank the Cellular and Molecular Imaging Core Facility (CMIC), Norwegian University of Science and

869 Technology (NTNU) for guidance and help during the acquisition of the TEM images. CMIC is
870 funded by the Faculty of Medicine at NTNU and Central Norway Regional Health Authority.

871

872 **TABLES:**

873

874 **Table 1. Photosystem absorption cross-section and Chl *a* content per P700 in *alb3b* mutants**
875 **compared to WT cells.** Photosystem absorption cross-section was measured as rate of 533 nm (Fx)
876 or 670 nm (Chl *a*) photons absorbed by the functional thylakoid membranes. The actinic light
877 intensity was adjusted to I_{670} = 2.1 µmol photons m^{-2} s^{-1} and I_{533} = 12 µmol photons m^{-2} s^{-1}. Rates of
878 light absorption and utilization are given in photons per second with ±SD. P700 quantification was
879 measured from the light induced ΔA_{700} with 670 nm (Chl *a*) actinic illumination.
880

		WT	*alb3b-14*	*alb3b-16*	*alb3b-19*	Average *alb3b*	*alb3b*/WT %
PSI	**(Fx) 533 nm**	**2.61 s $^{-1}$** ± 0.40	1.10 ± 0.08	1.17 ± 0.10	1.09 ± 0.00	**1.10 ± 0.06 s $^{-1}$**	**42 %**
	(Chl) 670 nm	**1.93 s $^{-1}$** ± 0.11	1.43 ± 0.05	1.39 ± 0.15	1.39 ± 0.14	**1.40 ± 0.01 s $^{-1}$**	**72.5%**
PSII	**(Fx) 533 nm**	**32.30 s $^{-1}$**± 0.7	13.92 ± 1.96	8.10 ± 1.16	8.58 ± 0.93	**10.17 ± 3.24 s $^{-1}$**	**35 %**
	(Chl) 670 nm	**12.62 s $^{-1}$** ± 2.69	7.21 ± 0.00	7.08 ± 0.90	6.71 ± 1.36	**7.00 ± 0.26 s $^{-1}$**	**55 %**
Chl *a* /P700		663±9 % : 1	466 ± 11 %	414 ± 9 %	394 ± 11 %	425:1	**64%**

881

882

Table 2. Photosynthesis and respiration properties of the WT and the *alb3b* KO lines. Parameters are calculated from the light-saturation curves of photosynthesis based on oxygen evolution of WT and *alb3b* KO lines (Figure 7; LL: Figure 7E, ML: Figure 7F). Data for *alb3b* are presented as an average of the three independent *alb3b* KO (*alb3b-14*, *alb3b-16, alb3b-19*) lines ±SD. A minimum of three biological replicates were measured for each independent line.

	LL		ML	
	WT	***alb3b***	**WT**	***alb3b***
Respiration (µmol O_2/ mol Chl/s)	30.0 ± 13.6	23.8 ± 1.7	23.5 ± 5.9	24.9 ± 3.2
P_{max} (µmol O_2/ mol Chl/s)	57.7 ± 11.5	63.2 ± 3.1	55.7 ± 4.9	71.8 ± 7.6
E_s (Saturation intensity, µmol photons m^{-2} s^{-1})	96.5	250	170	> 400
Maximum light utilization coefficient (α)	0.35	0.32	0.29	0.25

Table 3. Growth rates of WT and *alb3b* mutant lines acclimated to different light intensities. Maximum cell division per day were calculated from three biological replicates of WT and *alb3b* KO lines acclimated to LL (35 µmol photons m^{-2} s^{-1}), ML (200 µmol photons m^{-2} s^{-1}), or HL (480 µmol photons m^{-2} s^{-1}). Values are presented with ±SD. Growth rate for the *alb3b-16* mutant in HL was not calculated because of cell aggregation.

	WT	***alb3b-14***	***alb3b-16***	***alb3b-19***	***alb3b* average**
LL	1.6 ± 0.23	0.4 ± 0.02	0.6 ± 0.02	0.6 ± 0.03	0.5 ± 0.09
ML	2.2 ± 0.03	1.1 ± 0.01	1.2 ± 0.03	1.4 ± 0.05	1.2 ± 0.13
HL	2.0 ± 0.05	0.8 ± 0.17	n/a	0.9 ± 0.25	0.8 ± 0.19

FIGURE LEGENDS:

Figure 1: Presentation of intact and truncated ALB3b protein. A) The area of the ALB3b protein corresponding to the 20 bp target region for CRISPR/Cas9-based gene editing is located toward the N-terminal part of the protein (blue highlighting) with the PAM site located at the reverse DNA strand (green highlighting). CTP: Chloroplast targeting peptide; 60 kD IMP: 60 kD Inner Membrane Protein domain; CTD: conserved C-terminal domain. B) Overview of amino acid sequences resulting from CRISPR/Cas9 induced inserts in the three *alb3b* KO lines causing premature stop codons and truncated ALB3b proteins. Color coding: Blue: WT target sequence; Green: amino acid corresponding to PAM site; Red letters: Insert; *: Premature stop. C) Protein alignment based on the C-terminal domain (CTD) of ALB3b proteins in diatoms.

Figure 2. Color differences and spectral characteristics of WT and *alb3b* mutants. A) Visual representation of the *alb3b* phenotype compared to WT at low light (LL; 35 µmol photons m^{-2} s^{-1}; left side) and medium light (ML; 200 µmol photons m^{-2} s^{-1}; right side). For comparison and visualization of the color differences, all cultures were adjusted to equal cell densities (3 x 10^7 cells/ml). B) Absorbance spectra and C) *in vivo* fluorescence excitation spectra of cultures acclimated to ML. Isolated intact thylakoid membranes were used for recording of the absorption spectra to avoid scattering. Fluorescence emission was measured at 730 nm to ensure origin from the reaction center II Chl *a*. Insets: Difference spectra between: the absorbance of WT and *alb3b* KO lines B) and excitation energy transfer in the blue-green region of the *in vivo* fluorescence excitation spectra C). WT: Presented as an average of three biological replicates; *alb3b*: Presented as an average of the three *alb3b* KO lines 14, 16, and 19 with ±SD for all data points indicated by the grey area around the graphs. Three biological replicates were measured for each line.

Figure 3. 77 K fluorescence emission spectra of WT and *alb3b* KO samples acclimated to ML. Samples were excited at either A) 435 nm or B) 470 nm. The emission spectra were normalized at their 710 nm maximum. Data for *alb3b* is an average of the three *alb3b* KO lines 14, 16, and 19 with ±SD for all data points indicated by the grey area around the graphs. Three biological replicates were measured for each line including the WT.

Figure 4. Western blot analysis of thylakoid membrane proteins from WT and *alb3b* mutant lines acclimated to LL or ML conditions. A) Abundance of LHC proteins belonging to the LHCF group were evaluated using an antibody recognizing LHCF1-11, whereas the LHCX proteins were recognized by anti-FCP6 (a LHCX family member of *C. meneghiniana*). A dilution series of the WT samples was used to assess the level of LHC proteins in *alb3b* mutants compared to WT. B) Protein expression of PSII and PSI core proteins were evaluated with antibodies against the D1 (PSII), D2 (PSII), and PsaC (PSI) core subunits. A dilution series of the *alb3b* samples were used to assess the level of photosystem subunits in *alb3b* mutants compared to WT. An antibody recognizing the β-subunit of ATP synthase (AtpB) were used as loading control on each of the individual blots. Lanes marked with 100% contain 10 µg (20 µg for analysis of LHCX levels) of protein extracts. Images have been cropped.

Figure 5. Pigment concentrations per cell for WT and *alb3b* mutant lines as a function of ML exposure time. Cellular pigment concentrations of A) Chl *a*, B) Fx, C) Ddx, and D) Dtx in WT and *alb3b* mutant cells as a function of time following a shift from LL conditions (0 h; 35 µmol photons m^{-2} s^{-1}) to ML conditions (200 µmol photons m^{-2} s^{-1}) for 0.5, 6, 24, 48, and 168 h. Results are presented as a mean of three biological replicates with ±SD. Asterisks indicate the results of two-tailed Student *t*-tests: *$p<0.05$.

Figure 6. De-epoxidation state index and NPQ capacity of WT and *alb3b* mutants. A) De-epoxidation state index (DES = Dtx/(Dtx + Ddx)) calculated from the HPLC pigment data from LL acclimated (0 h) WT and *alb3b* cultures exposed to ML for 0.5, 6, 24, 48, and 168 h. B) Capacity for NPQ calculated from rapid light curves derived from LL-acclimated cells approx. two months after isolation of mutated single cells and C) after being maintained in culture for one more year. NPQ = $(F_{m'max}/F_{m'}) - 1$. $F_{m'max}$ replaces the commonly used F_m since $F_{m'}$ values frequently occur that are higher than the F_m from dark-treated diatom samples (Serôdio et al., 2006). Results are presented as a mean of three biological replicates with ±SD.

Figure 7. Photo-physiological responses of WT and *alb3b* mutant lines. *In vivo* Chl *a* fluorescence kinetics (PAM) were used to estimate A) the maximum quantum yield of PSII (F_v/F_m), B) the

maximum light utilization coefficient (α), C) the maximum relative light-saturated electron transport rate ($rETR_{max}$), and D) the light saturation index (E_k) in LL (0h) acclimated WT and *alb3b* KO lines as a function of ML exposure time (0.5-168 h). Values are presented with ±SD bars. Asterisks indicate the results of two-tailed Student *t*-tests: *p<0.05. Light-saturation curves of photosynthesis based on oxygen evolution were produced for E) LL-acclimated and F) ML-acclimated WT and *alb3b* KO lines. The oxygen concentration was normalized on a per-Chl basis. The results were fit with curves based on a polynomial regression using R. All values are presented as an average of three biological replicates for each line and ±SD for each value can be found in Supplemental Table S3.

Figure 8. Culture color, LHCF protein level, and pigment concentration in complemented *alb3b* lines compared to WT. A) WT and complemented *alb3b* KO lines (*alb3b-14C*, *alb3b-16C*, *alb3b-19C*) were acclimated to LL and ML conditions. All cultures were concentrated and adjusted to equal cell densities (3 x 10^7 cells/ml) for comparison. B) Western blot analysis of LHCF proteins in WT and complemented *alb3b* mutant lines acclimated to LL and ML conditions. LHCF protein levels were evaluated using LHCF1-11 antibody. An antibody recognizing the β-subunit of ATP synthase was used as loading control. 10 µg of total protein from cell lysates was loaded onto the gel. C) Cellular pigment concentrations of Chl *a* and Fx in LL conditions. Results are presented as a mean of three biological replicates with ±SD bars. Asterisks indicate the results of two-tailed Student *t*-tests: *p<0.05.

Figure 9. Proposed model of the role of diatom ALB3 insertases in insertion/assembly of thylakoid membrane proteins. LHC proteins are synthesized on ribosomes on the cERM, transported through the four membranes surrounding the secondary plastid of diatoms, and guided to ALB3b by an unknown protein complex before incorporation into the thylakoid membrane (left side). Chloroplast-encoded proteins are suggested to be integrated by the co-translational cpSRP pathway including cpSRP54, FTSY, and ALB3ba (right side). cERM: chloroplast ER membrane; PPM: periplastidal membrane; OEM: plastid outer envelope membrane; IEM: plastid inner envelope membrane. CpSRP54: chloroplast signal recognition particle protein 54; CpFTSY: chloroplast SRP

receptor; ALB3: chloroplast SRP insertase Albino3.

REFERENCES

Ago H, Adachi H, Umena Y, Tashiro T, Kawakami K, Kamiya N, Tian L, Han G, Kuang T, Liu Z, Wang F, Zou H, Enami I, Miyano M, Shen JR (2016) Novel features of eukaryotic photosystem II revealed by its crystal structure analysis from a red alga. J Biol Chem **291:** 5676-5687

Armbrust EV, Berges JA, Bowler C, Green BR, Martinez D, Putnam NH, Zhou S, Allen AE, Apt KE, Bechner M, Brzezinski MA, Chaal BK, Chiovitti A, Davis AK, Demarest MS, Detter JC, Glavina T, Goodstein D, Hadi MZ, Hellsten U, Hildebrand M, Jenkins BD, Jurka J, Kapitonov VV, Kroger N, Lau WW, Lane TW, Larimer FW, Lippmeier JC, Lucas S, Medina M, Montsant A, Obornik M, Parker MS, Palenik B, Pazour GJ, Richardson PM, Rynearson TA, Saito MA, Schwartz DC, Thamatrakoln K, Valentin K, Vardi A, Wilkerson FP, Rokhsar DS (2004) The genome of the diatom *Thalassiosira pseudonana*: ecology, evolution, and metabolism. Science **306:** 79-86

Austin JR, 2nd, Staehelin LA (2011) Three-dimensional architecture of grana and stroma thylakoids of higher plants as determined by electron tomography. Plant Physiol **155:** 1601-1611

Bailleul B, Rogato A, de Martino A, Coesel S, Cardol P, Bowler C, Falciatore A, Finazzi G (2010) An atypical member of the light-harvesting complex stress-related protein family modulates diatom responses to light. Proc Natl Acad Sci U S A **107:** 18214-18219

Baroli I, Melis A (1996) Photoinhibition and repair in *Dunaliella salina* acclimated to different growth irradiances. Planta **198:** 640-646

Bellafiore S, Ferris P, Naver H, Gohre V, Rochaix JD (2002) Loss of Albino3 leads to the specific depletion of the light-harvesting system. Plant Cell **14:** 2303-2314

Ben-Shem A, Frolow F, Nelson N (2003) Crystal structure of plant photosystem I. Nature **426:** 630-635

Bowler C, Allen AE, Badger JH, Grimwood J, Jabbari K, Kuo A, Maheswari U, Martens C, Maumus F, Otillar RP, Rayko E, Salamov A, Vandepoele K, Beszteri B, Gruber A, Heijde M, Katinka M, Mock T, Valentin K, Verret F, Berges JA, Brownlee C, Cadoret JP, Chiovitti A, Choi CJ, Coesel S, De Martino A, Detter JC, Durkin C, Falciatore A, Fournet J, Haruta M, Huysman MJ, Jenkins BD, Jiroutova K, Jorgensen RE, Joubert Y, Kaplan A, Kroger N, Kroth PG, La Roche J, Lindquist E, Lommer M, Martin-Jezequel V, Lopez PJ, Lucas S, Mangogna M, McGinnis K, Medlin LK, Montsant A, Oudot-Le Secq MP, Napoli C, Obornik M, Parker MS, Petit JL, Porcel BM, Poulsen N, Robison M, Rychlewski L, Rynearson TA, Schmutz J, Shapiro H, Siaut M, Stanley M, Sussman MR, Taylor AR, Vardi A, von Dassow P, Vyverman W, Willis A, Wyrwicz LS, Rokhsar DS, Weissenbach J, Armbrust EV, Green BR, Van de Peer Y, Grigoriev IV (2008) The *Phaeodactylum* genome reveals the evolutionary history of diatom genomes. Nature **456:** 239-244

Bozzola JJ, Russell LD (1999) Electron Microscopy: Principles and Techniques for Biologists, Second Edition, Jones and Bartlett, Boston, Publishers.

Bricaud A, Claustre H, Ras J, Oubelkheir K (2004) Natural variability of phytoplanktonic absorption in oceanic waters: Influence of the size structure of algal populations. J Geophys Res-Oceans **109**

Brown JW, Sorhannus U (2010) A molecular genetic timescale for the diversification of autotrophic stramenopiles (Ochrophyta): substantive underestimation of putative fossil ages. PLoS One **5**

Büchel C (2014) Fucoxanthin-Chlorophyll-proteins and non-photochemical fluorescence quenching of diatoms. *In* B Demmig-Adams, G Garab, W Adams III, Govindjee, eds, Non-photochemical quenching and energy dissipation in plants, algae and cyanobacteria. Advances in photosynthesis and respiration (Including bioenergy and related processes), Vol 40. Springer, Dordrecht

Büchel C (2015) Evolution and function of light harvesting proteins. J Plant Physiol **172:** 62-75

Chandrasekar S, Shan SO (2017) Anionic phospholipids and the Albino3 translocase activate signal recognition particle-receptor interaction during light-harvesting chlorophyll *a/b*-binding protein targeting. J Biol Chem **292:** 397-406

Cruz S, Goss R, Wilhelm C, Leegood R, Horton P, Jakob T (2011) Impact of chlororespiration on non-photochemical quenching of chlorophyll fluorescence and on the regulation of the diadinoxanthin cycle in the diatom *Thalassiosira pseudonana*. J Exp Bot **62:** 509-519

Cruz S, Serôdio J (2008) Relationship of rapid light curves of variable fluorescence to photoacclimation and non-photochemical quenching in a benthic diatom. Aquat Bot **88:** 256-264

De Martino A, Bartual A, Willis A, Meichenin A, Villazan B, Maheswari U, Bowler C (2011) Physiological and molecular evidence that environmental changes elicit morphological interconversion in the model diatom *Phaeodactylum tricornutum*. Protist **162:** 462-481

De Martino A, Meichenin A, Shi J, Pan KH, Bowler C (2007) Genetic and phenotypic characterization of *Phaeodactylum tricornutum* (Bacillariophyceae) accessions. J Phycol **43:** 992-1009

Durnford DG, Aebersold R, Green BR (1996) The fucoxanthin-chlorophyll proteins from a chromophyte alga are part of a large multigene family: structural and evolutionary relationships to other light harvesting antennae. Mol Gen Genet **253:** 377-386

Dünschede B, Bals T, Funke S, Schunemann D (2011) Interaction studies between the chloroplast signal recognition particle subunit cpSRP43 and the full-length translocase Alb3 reveal a membrane-embedded binding region in Alb3 protein. J Biol Chem **286:** 35187-35195

Falk S, Ravaud S, Koch J, Sinning I (2010) The C terminus of the Alb3 membrane insertase recruits cpSRP43 to the thylakoid membrane. J Biol Chem **285:** 5954-5962

Falk S, Sinning I (2010) The C terminus of Alb3 interacts with the chromodomains 2 and 3 of cpSRP43. J Biol Chem **285:** le25-26; author reply le26-28

Falkowski PG, Barber RT, Smetacek V (1998) Biogeochemical controls and feedbacks on ocean primary production. Science **281:** 200-206

Falkowski PG, Raven JA (2007) Aquatic photosynthesis, Ed Second edition. Princeton University Press, Princeton

Fawley MW (1984) Effects of llight intensity and temperature interactions on growth characteristics of *Phaeodactylum tricornutum* (Bacillariophyceae). J Phycol **20:** 67-72

Formighieri C, Melis A (2017) Heterologous synthesis of geranyllinalool, a diterpenol plant product, in the cyanobacterium Synechocystis. Appl Microbiol Biotechnol **101:** 2791-2800

Genty B, Briantais JM, Baker NR (1989) The relationship between the quantum yield of

photosynthetic electron-transport and quenching of chlorophyll fluorescence. Biochim Biophys Acta **990:** 87-92

Gerdes L, Bals T, Klostermann E, Karl M, Philippar K, Hunken M, Soll J, Schunemann D (2006) A second thylakoid membrane-localized Alb3/OxaI/YidC homologue is involved in proper chloroplast biogenesis in *Arabidopsis thaliana*. J Biol Chem **281:** 16632-16642

Giovagnetti V, Ruban AV (2017) Detachment of the fucoxanthin chlorophyll *a/c* binding protein (FCP) antenna is not involved in the acclimative regulation of photoprotection in the pennate diatom *Phaeodactylum tricornutum*. Biochim Biophys Acta **1858:** 218-230

Goss R, Lepetit B (2015) Biodiversity of NPQ. J Plant Physiol **172:** 13-32

Grouneva I, Rokka A, Aro EM (2011) The thylakoid membrane proteome of two marine diatoms outlines both diatom-specific and species-specific features of the photosynthetic machinery. J Proteome Res **10:** 5338-5353

Gu J, Zhou Z, Li Z, Chen Y, Wang Z, Zhang H, Yang J (2017) Photosynthetic properties and potentials for improvement of photosynthesis in pale green leaf rice under high light conditions. Front Plant Sci **8:** 1082

Guenther JE, Melis A (1990) The physiological significance of photosystem II heterogeneity in chloroplasts. Photosynth Res **23:** 105-109

Guillard RR, Ryther JH (1962) Studies of marine planktonic diatoms. I. Cyclotella nana Hustedt, and Detonula confervacea (cleve) Gran. Can J Microbiol **8:** 229-239

Gundermann K, Büchel C (2014) Structure and functional heterogeneity of fucoxanthin-chlorophyll proteins in diatoms. *In* M Hohmann-Marriott, ed, The Structural Basis of Biological Energy Generation. Advances in Photosynthesis and Respiration (Including Bioenergy and Related Processes), Vol 39. Springer Dordrecht

Göhre V, Ossenbuhl F, Crevecoeur M, Eichacker LA, Rochaix JD (2006) One of two alb3 proteins is essential for the assembly of the photosystems and for cell survival in *Chlamydomonas*. Plant Cell **18:** 1454-1466

Havaux M, Dall'Osto L, Bassi R (2007) Zeaxanthin has enhanced antioxidant capacity with respect to all other xanthophylls in *Arabidopsis* leaves and functions independent of binding to PSII antennae. Plant Physiol **145:** 1506-1520

Hennon SW, Soman R, Zhu L, Dalbey RE (2015) YidC/Alb3/Oxa1 family of insertases. J Biol Chem **290:** 14866-14874

Herbstova M, Bina D, Kana R, Vacha F, Litvin R (2017) Red-light phenotype in a marine diatom involves a specialized oligomeric red-shifted antenna and altered cell morphology. Sci Rep **7:** 11976

Hiyama T, Ke B (1972) Difference spectra and extinction coefficients of P700. Biochim Biophys Acta **267:** 160-171

Ikeda Y, Komura M, Watanabe M, Minami C, Koike H, Itoh S, Kashino Y, Satoh K (2008) Photosystem I complexes associated with fucoxanthin-chlorophyll-binding proteins from a marine centric diatom, *Chaetoceros gracilis*. Biochim Biophys Acta **1777:** 351-361

Jeffrey SW, Humphrey GF (1975) New spectrophotometric equations for determining chlorophylls *a*, *b*, *c1* and *c2* in higher plants, algae and natural phytoplankton. Biochem Physiol Pfl **167:** 191-194

Juhas M, Buchel C (2012) Properties of photosystem I antenna protein complexes of the diatom *Cyclotella meneghiniana*. J Exp Bot **63:** 3673-3681

Juhas M, von Zadow A, Spexard M, Schmidt M, Kottke T, Buchel C (2014) A novel cryptochrome in the diatom *Phaeodactylum tricornutum* influences the regulation of light-harvesting protein levels. Febs J **281:** 2299-2311

Kalaji HM, Schansker G, Brestic M, Bussotti F, Calatayud A, Ferroni L, Goltsev V, Guidi L, Jajoo A, Li P, Losciale P, Mishra VK, Misra AN, Nebauer SG, Pancaldi S, Penella C, Pollastrini M, Suresh K, Tambussi E, Yanniccari M, Zivcak M, Cetner MD, Samborska IA, Stirbet A, Olsovska K, Kunderlikova K, Shelonzek H, Rusinowski S, Baba W (2017) Frequently asked questions about chlorophyll fluorescence, the sequel. Photosynth Res **132:** 13-66

Kirst H, Formighieri C, Melis A (2014) Maximizing photosynthetic efficiency and culture productivity in cyanobacteria upon minimizing the phycobilisome light-harvesting antenna size. Bba-Bioenergetics **1837:** 1653-1664

Kirst H, Gabilly ST, Niyogi KK, Lemaux PG, Melis A (2017) Photosynthetic antenna engineering to improve crop yields. Planta **245:** 1009-1020

Kirst H, Garcia-Cerdan JG, Zurbriggen A, Melis A (2012) Assembly of the light-harvesting chlorophyll antenna in the green alga *Chlamydomonas reinhardtii* requires expression of the TLA2-CpFTSY gene. Plant Physiol **158:** 930-945

Kirst H, Garcia-Cerdan JG, Zurbriggen A, Ruehle T, Melis A (2012) Truncated photosystem chlorophyll antenna size in the green microalga *Chlamydomonas reinhardtii* upon deletion of the TLA3-CpSRP43 gene. Plant Physiol **160:** 2251-2260

Kirst H, Melis A (2014) The chloroplast signal recognition particle (CpSRP) pathway as a tool to minimize chlorophyll antenna size and maximize photosynthetic productivity. Biotechnol Adv **32:** 66-72

Kirst H, Shen Y, Vamvaka E, Betterle N, Xu D, Warek U, Strickland JA, Melis A (2018) Downregulation of the CpSRP43 gene expression confers a truncated light-harvesting antenna (TLA) and enhances biomass and leaf-to-stem ratio in *Nicotiana tabacum* canopies. Planta **248:** 139-154

Kugelmann M, Fausser A, Ossenbuhl F, Brennicke A (2013) Phenotypes of Alb3p and carotenoid synthesis mutants show similarities regarding light sensitivity, thylakoid structure and protein stability. Photosynthetica **51:** 45-54

Kumar S, Stecher G, Tamura K (2016) MEGA7: Molecular Evolutionary Genetics Analysis Version 7.0 for Bigger Datasets. Mol Biol Evol **33:** 1870-1874

Lamb J, Forfang K, Hohmann-Marriott M (2015) A practical solution for 77 K fluorescence measurements based on LED excitation and CCD array detector. PLoS One **10:** e0132258

Lang M, Kroth PG (2001) Diatom fucoxanthin chlorophyll a/c-binding protein (FCP) and land plant light-harvesting proteins use a similar pathway for thylakoid membrane Insertion. J Biol Chem **276:** 7985-7991

Lavaud J, Goss R (2014) The peculiar features of non-photochemical fluorescence quenching in diatoms and brown algae. *In* B Demmig-Adams, G Garab, IW Adams, Govindjee, eds, Non-photochemical quenching and energy dissipation in plants, algae and cyanobacteria. Advances in photosynthesis and respiration (Including bioenergy and related processes), Vol 40. Springer, Dordrecht

Lavaud J, Lepetit B (2013) An explanation for the inter-species variability of the photoprotective non-photochemical chlorophyll fluorescence quenching in diatoms. Biochim Biophys Acta **1827:** 294-302

Lavaud J, Rousseau B, van Gorkom HJ, Etienne AL (2002) Influence of the diadinoxanthin pool size on photoprotection in the marine planktonic diatom *Phaeodactylum tricornutum*. Plant Physiol **129:** 1398-1406

Le SQ, Gascuel O (2008) An improved general amino acid replacement matrix. Mol Biol Evol **25:** 1307-1320

Lepetit B, Gelin G, Lepetit M, Sturm S, Vugrinec S, Rogato A, Kroth PG, Falciatore A, Lavaud J (2017) The diatom *Phaeodactylum tricornutum* adjusts nonphotochemical fluorescence quenching capacity in response to dynamic light via fine-tuned Lhcx and xanthophyll cycle pigment synthesis. New Phytol **214:** 205-218

Lepetit B, Goss R, Jakob T, Wilhelm C (2012) Molecular dynamics of the diatom thylakoid membrane under different light conditions. Photosynth Res **111:** 245-257

Lepetit B, Sturm S, Rogato A, Gruber A, Sachse M, Falciatore A, Kroth PG, Lavaud J (2013) High light acclimation in the secondary plastids containing diatom *Phaeodactylum tricornutum* is triggered by the redox state of the plastoquinone pool. Plant Physiol **161:** 853-865

Lepetit B, Volke D, Gilbert M, Wilhelm C, Goss R (2010) Evidence for the existence of one antenna-associated, lipid-dissolved and two protein-bound pools of diadinoxanthin cycle pigments in diatoms. Plant Physiol **154:** 1905-1920

Lewis NE, Marty NJ, Kathir KM, Rajalingam D, Kight AD, Daily A, Kumar TK, Henry RL, Goforth RL (2010) A dynamic cpSRP43-Albino3 interaction mediates translocase regulation of chloroplast signal recognition particle (cpSRP)-targeting components. J Biol Chem **285:** 34220-34230

Madhuri S, Serif M, Rio Bartulos C, Lepetit B, Kroth PG (2019) A strategy to complement PtAUREO1a in TALEN knockout strains of *Phaeodactylum tricornutum*. Algal Res **39:** 101469

Melis A (1989) Spectroscopic methods in photosynthesis - Photosystem stoichiometry and chlorophyll antenna size. Philos T Roy Soc B **323:** 397-409

Melis A, Brown JS (1980) Stoichiometry of system I and system II reaction centers and of plastoquinone in different photosynthetic membranes. P Natl Acad Sci-Biol **77:** 4712-4716

Miloslavina Y, Grouneva I, Lambrev PH, Lepetit B, Goss R, Wilhelm C, Holzwarth AR (2009) Ultrafast fluorescence study on the location and mechanism of non-photochemical quenching in diatoms. Biochim Biophys Acta **1787:** 1189-1197

Mock T, Otillar RP, Strauss J, McMullan M, Paajanen P, Schmutz J, Salamov A, Sanges R, Toseland A, Ward BJ, Allen AE, Dupont CL, Frickenhaus S, Maumus F, Veluchamy A, Wu T, Barry KW, Falciatore A, Ferrante MI, Fortunato AE, Glöckner G, Gruber A, Hipkin R, Janech MG, Kroth PG, Leese F, Lindquist EA, Lyon BR, Martin J, Mayer C, Parker M, Quesneville H, Raymond JA, Uhlig C, Valas RE, Valentin KU, Worden AZ, Armbrust EV, Clark MD, Bowler C, Green BR, Moulton V, van Oosterhout C, Grigoriev IV (2017) Evolutionary genomics of the cold-adapted diatom *Fragilariopsis cylindrus*. Nature **541:** 536

Moore M, Harrison MS, Peterson EC, Henry R (2000) Chloroplast Oxa1p homolog albino3 is required for post-translational integration of the light harvesting chlorophyll-binding protein into thylakoid membranes. J Biol Chem **275:** 1529-1532

Nelson N, Yocum CF (2006) Structure and function of photosystems I and II. Annu Rev Plant Biol **57:** 521-565

Nicholas KB, Nicholas HBJ, Deerfield DWI (1997) GeneDoc: analysis and visualization of genetic variation. EMBNEW. NEWS **4**

Nymark M, Sharma AK, Hafskjold MC, Sparstad T, Bones AM, Winge P (2017) CRISPR/Cas9 Gene editing in the marine diatom *Phaeodactylum tricornutum*. Bio-protocol **7:** e2442

Nymark M, Sharma AK, Sparstad T, Bones AM, Winge P (2016) A CRISPR/Cas9 system adapted for gene editing in marine algae. Sci Rep-Uk **6**

Nymark M, Valle KC, Brembu T, Hancke K, Winge P, Andresen K, Johnsen G, Bones AM

(2009) An integrated analysis of molecular acclimation to high light in the marine diatom *Phaeodactylum tricornutum*. PLoS ONE **4:** e7743

Nymark M, Valle KC, Hancke K, Winge P, Andresen K, Johnsen G, Bones AM, Brembu T (2013) Molecular and photosynthetic responses to prolonged darkness and subsequent acclimation to re-illumination in the diatom *Phaeodactylum tricornutum*. PLoS ONE **8:** e58722

Oey M, Ross IL, Stephens E, Steinbeck J, Wolf J, Radzun KA, Kugler J, Ringsmuth AK, Kruse O, Hankamer B (2013) RNAi knock-down of LHCBM1, 2 and 3 Increases photosynthetic H_2 production efficiency of the green alga *Chlamydomonas reinhardtii*. Plos One **8**

Ossenbühl F, Gohre V, Meurer J, Krieger-Liszkay A, Rochaix JD, Eichacker LA (2004) Efficient assembly of photosystem II in *Chlamydomonas reinhardtii* requires Alb3.1p, a homolog of *Arabidopsis* ALBINO3. Plant Cell **16:** 1790-1800

Oudot-Le Secq MP, Grimwood J, Shapiro H, Armbrust EV, Bowler C, Green BR (2007) Chloroplast genomes of the diatoms *Phaeodactylum tricornutum* and *Thalassiosira pseudonana*: comparison with other plastid genomes of the red lineage. Mol Genet Genomics **277:** 427-439

Polle JE, Kanakagiri SD, Melis A (2003) Tla1, a DNA insertional transformant of the green alga *Chlamydomonas reinhardtii* with a truncated light-harvesting chlorophyll antenna size. Planta **217:** 49-59

Powles SB, Critchley C (1980) Effect of light intensity during growth on photoinhibition of intact attached bean leaflets. Plant Physiol **65:** 1181-1187

Premvardhan L, Bordes L, Beer A, Büchel C, Robert B (2009) Carotenoid structures and environments in trimeric and oligomeric fucoxanthin chlorophyll *a*/c_2 proteins from resonance Raman spectroscopy. J Phys Chem B **113:** 12565-12574

Premvardhan L, Robert B, Beer A, Büchel C (2010) Pigment organization in fucoxanthin chlorophyll *a*/c_2 proteins (FCP) based on resonance Raman spectroscopy and sequence analysis. Biochim Biophys Acta **1797:** 1647-1656

Ramakers C, Ruijter JM, Deprez RH, Moorman AF (2003) Assumption-free analysis of quantitative real-time polymerase chain reaction (PCR) data. Neurosci Lett **339:** 62-66

Rodriguez F, Chauton M, Johnsen G, Andresen K, Olsen LM, Zapata M (2006) Photoacclimation in phytoplankton: implications for biomass estimates, pigment functionality and chemotaxonomy. Mar Biol **148:** 963-971

Ruijter JM, Ramakers C, Hoogaars WM, Karlen Y, Bakker O, van den Hoff MJ, Moorman AF (2009) Amplification efficiency: linking baseline and bias in the analysis of quantitative PCR data. Nucleic Acids Res **37:** e45

Saitou N, Nei M (1987) The neighbor-joining method: a new method for reconstructing phylogenetic trees. Mol Biol Evol **4:** 406-425

Sakshaug E, Bricaud A, Dandonneau Y, Falkowski PG, Kiefer DA, Legendre L, Morel A, Parslow J, Takahashi M (1997) Parameters of photosynthesis: definitions, theory and interpretation of results. J Plankton Res **19:** 1637-1670

Schuenemann D, Gupta S, Persello-Cartieaux F, Klimyuk VI, Jones JD, Nussaume L, Hoffman NE (1998) A novel signal recognition particle targets light-harvesting proteins to the thylakoid membranes. Proc Natl Acad Sci U S A **95:** 10312-10316

Serif M, Lepetit B, Weißert K, Kroth PG, Rio Bartulos C (2017) A fast and reliable strategy to generate TALEN-mediated gene knockouts in the diatom Phaeodactylum tricornutum. Algal Res 23: 186-195

Serôdio J, Vieira S, Cruz S, Coelho H (2006) Rapid light-response curves of chlorophyll

fluorescence in microalgae: relationship to steady-state light curves and non-photochemical quenching in benthic diatom-dominated assemblages. Photosynth Res **90:** 29-43

Sundberg E, Slagter JG, Fridborg I, Cleary SP, Robinson C, Coupland G (1997) ALBINO3, an Arabidopsis nuclear gene essential for chloroplast differentiation, encodes a chloroplast protein that shows homology to proteins present in bacterial membranes and yeast mitochondria. Plant Cell **9:** 717-730

Taddei L, Chukhutsina VU, Lepetit B, Stella GR, Bassi R, van Amerongen H, Bouly JP, Jaubert M, Finazzi G, Falciatore A (2018) Dynamic changes between two LHCX-related energy quenching sites control diatom photoacclimation. Plant Physiol **177:** 953-965

Taddei L, Stella GR, Rogato A, Bailleul B, Fortunato AE, Annunziata R, Sanges R, Thaler M, Lepetit B, Lavaud J, Jaubert M, Finazzi G, Bouly JP, Falciatore A (2016) Multisignal control of expression of the LHCX protein family in the marine diatom *Phaeodactylum tricornutum*. J Exp Bot **67:** 3939-3951

Theis J, Schroda M (2016) Revisiting the photosystem II repair cycle. Plant Signal Behav **11:** e1218587

Thompson JD, Gibson TJ, Plewniak F, Jeanmougin F, Higgins DG (1997) The CLUSTAL_X windows interface: flexible strategies for multiple sequence alignment aided by quality analysis tools. Nucleic Acids Res **25:** 4876-4882

Träger C, Rosenblad MA, Ziehe D, Garcia-Petit C, Schrader L, Kock K, Richter CV, Klinkert B, Narberhaus F, Herrmann C, Hofmann E, Aronsson H, Schunemann D (2012) Evolution from the prokaryotic to the higher plant chloroplast signal recognition particle: the signal recognition particle RNA is conserved in plastids of a wide range of photosynthetic organisms. Plant Cell **24:** 4819-4836

Valle KC, Nymark M, Aamot I, Hancke K, Winge P, Andresen K, Johnsen G, Brembu T, Bones AM (2014) System responses to equal doses of photosynthetically usable radiation of blue, green, and red light in the marine diatom Phaeodactylum tricornutum. PLoS One **9:** e114211

Yamagishi A, Ikeda Y, Komura M, Koike H, Satoh K, Itoh S, Shibata Y (2010) Shallow sink in an antenna pigment system of photosystem I of a marine centric diatom, *Chaetoceros gracilis*, revealed by ultrafast fluorescence spectroscopy at 17 K. J Phys Chem B **114:** 9031-9038

Wang W, Yu L-J, Xu C, Tomizaki T, Zhao S, Umena Y, Chen X, Qin X, Xin Y, Suga M, Han G, Kuang T, Shen J-R (2019) Structural basis for blue-green light harvesting and energy dissipation in diatoms. Science **363:** eaav0365

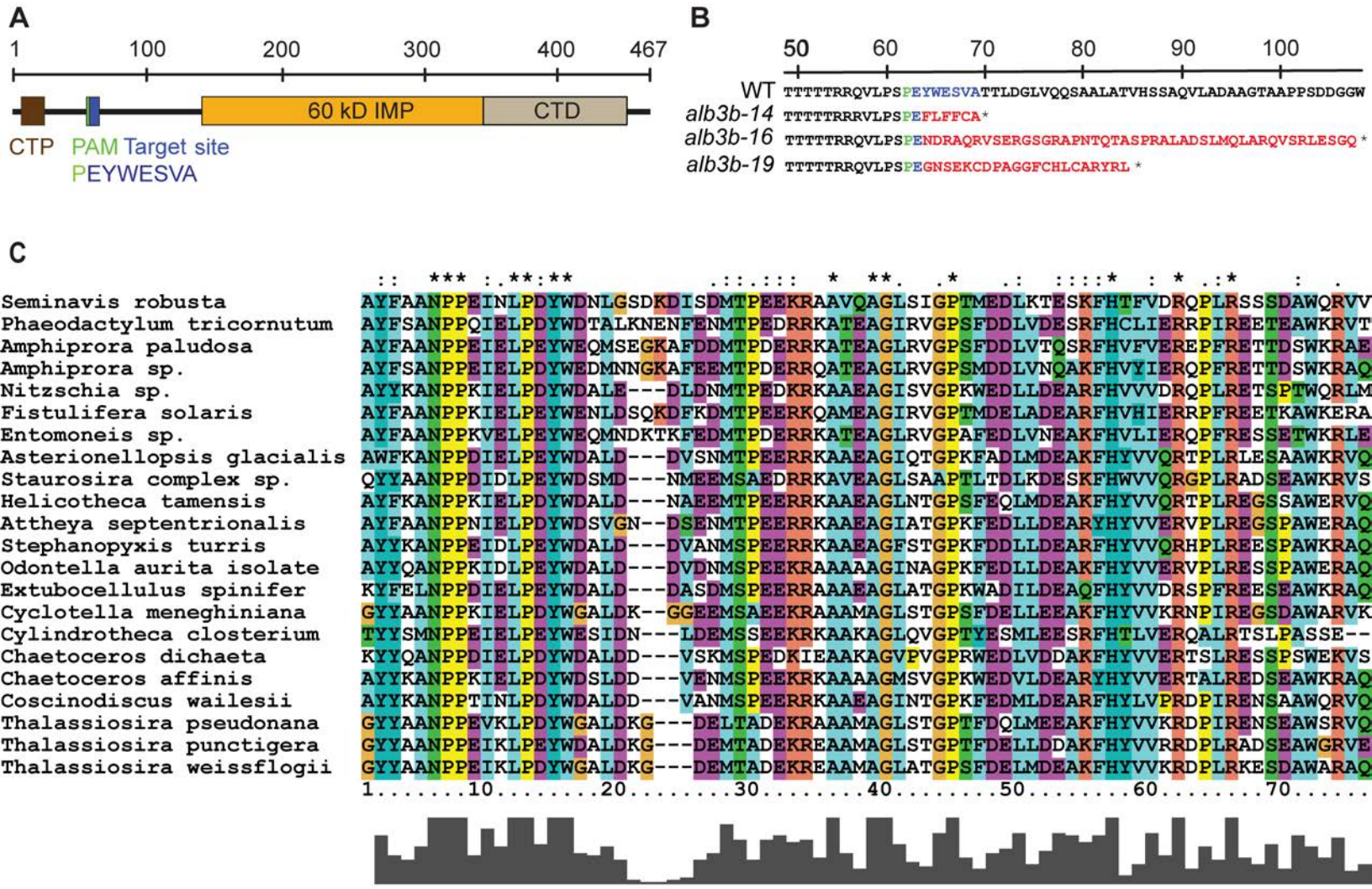

Figure 1: Presentation of intact and truncated ALB3b protein. A) The area of the ALB3b protein corresponding to the 20 bp target region for CRISPR/Cas9-based gene editing is located toward the N-terminal part of the protein (blue highlighting) with the PAM site located at the reverse DNA strand (green highlighting). CTP: Chloroplast targeting peptide; 60 kD IMP: 60 kD Inner Membrane Protein domain; CTD: conserved C-terminal domain. B) Overview of amino acid sequences resulting from CRISPR/Cas9 induced inserts in the three *alb3b* KO lines causing premature stop codons and truncated ALB3b proteins. Color coding: Blue: WT target sequence; Green: amino acid corresponding to PAM site; Red letters: Insert; *: Premature stop. C) Protein alignment based on the C-terminal domain (CTD) of ALB3b proteins in diatoms.

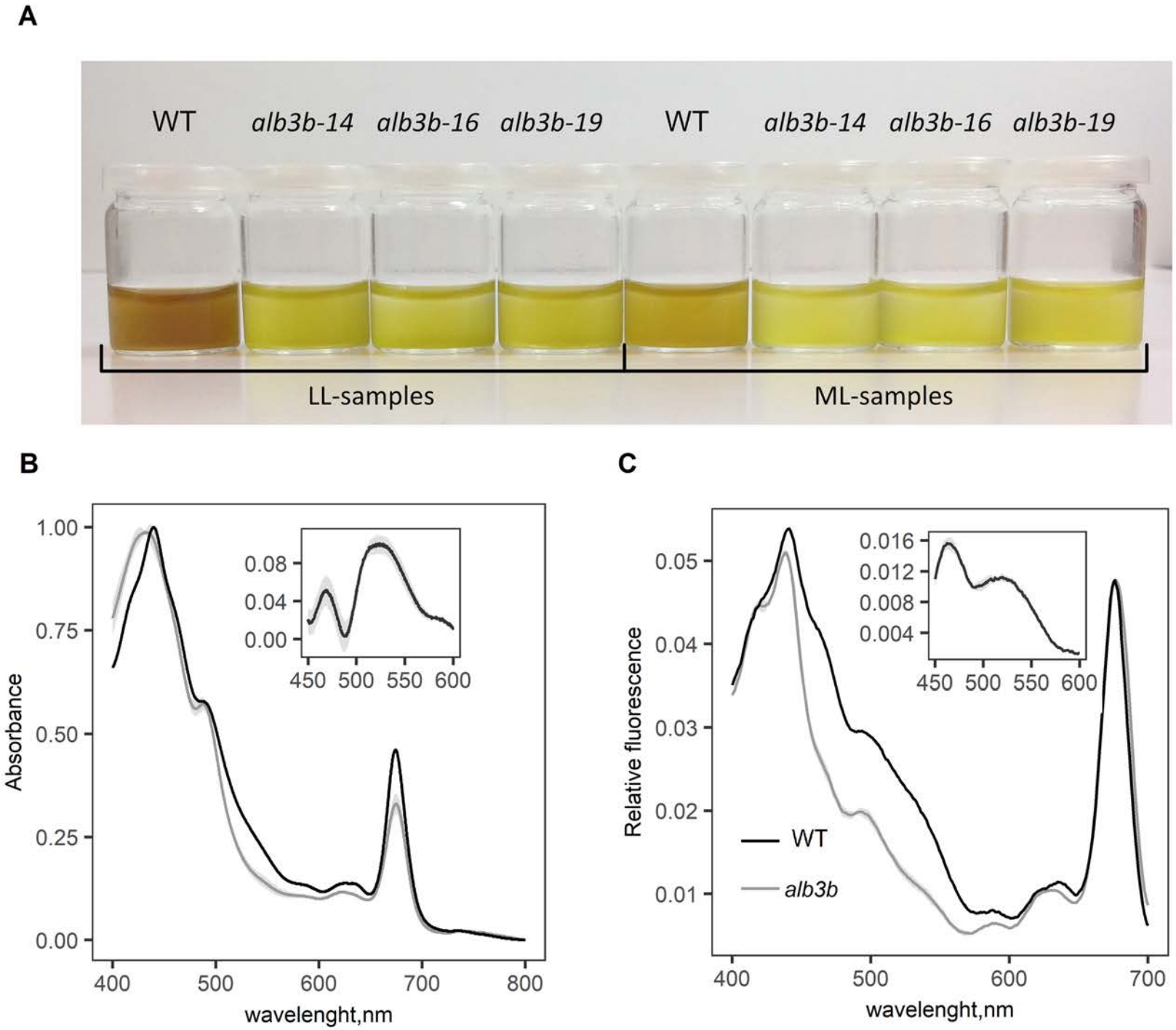

Figure 2. Color differences and spectral characteristics of WT and alb3b mutants. A) Visual representation of the *alb3b* phenotype compared to WT at low light (LL; 35 µmol photons m^{-2} s^{-1}; left side) and ML (200 µmol photons m^{-2} s^{-1}; right side). For comparison and visualization of the color differences, all cultures were adjusted to equal cell densities (3 x 10^7 cells/ml) B) Absorbance spectra and C) in vivo fluorescence excitation spectra of cultures acclimated to ML. Isolated intact thylakoid membranes were used for recording of the absorption spectra to avoid scattering. Fluorescence emission was measured at 730 nm to ensure origin from the reaction center II Chl *a*. Insets: Difference spectra between: the absorbance of WT and *alb3b* KO lines B), and excitation energy transfer in the blue-green region of the in vivo fluorescence excitation spectra C). WT: Presented as an average of three biological replicates; alb3b: Presented as an average of the three *alb3b* KO lines 14, 16 and 19 with ±SD for all data points indicated by the grey area around the graphs. Three biological replicates were measured for each line.

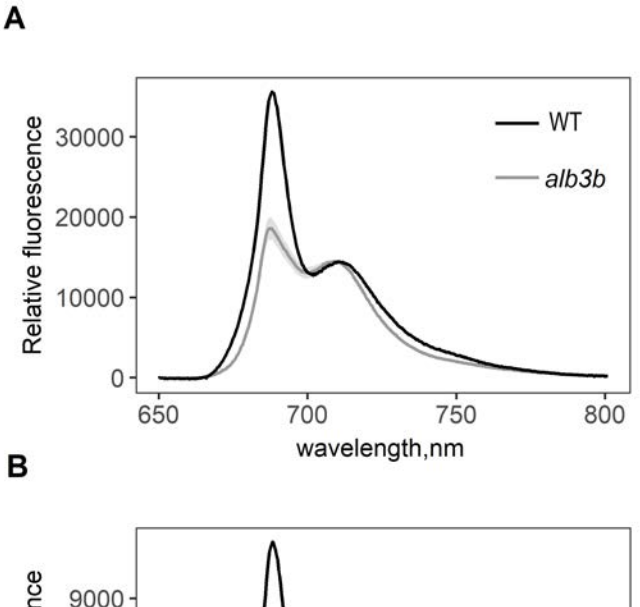

Figure 3. 77 K fluorescence emission spectra of WT and *alb3b* KO samples acclimated to ML. Samples were excited at either 435 nm (A) or 470 nm (B). The emission spectra were normalized at their 710 nm maximum. Data for alb3b is an average of the three *alb3b* KO lines 14, 16 and 19 with ±SD for all data points indicated by the grey area around the graphs. Three biological replicates were measured for each line including the WT.

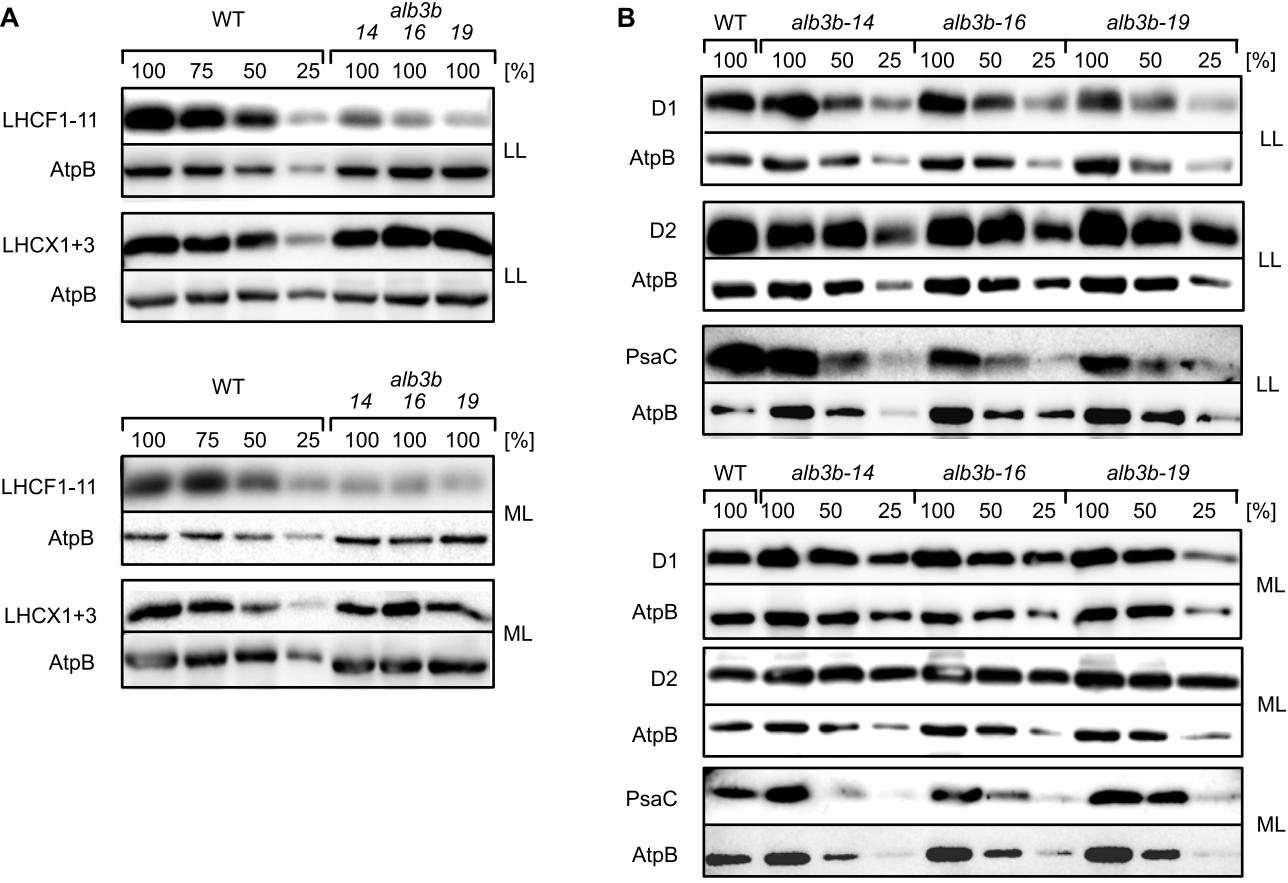

Figure 4. Western blot analysis of thylakoid membrane proteins from WT and *alb3b* mutant lines acclimated to LL or ML conditions. A) Abundance of LHC proteins belonging to the LHCF group were evaluated using an antibody recognizing LHCF1-11, whereas the LHCX proteins were recognized by anti-FCP6 (a LHCX family member of *C. meneghiniana*). A dilution series of the WT samples was used to assess the level of LHC proteins in *alb3b* mutants compared to WT. B) Protein expression of PSII and PSI core proteins were evaluated with antibodies against the D1 (PSII), D2 (PSII) and PsaC (PSI) core sub-units. A dilution series of the *alb3b* samples were used to assess the level of photosystem subunits in *alb3b* mutants compared to WT. An antibody recognizing the β-subunit of ATP synthase (AtpB) were used as loading control on each of the individual blots. Lanes marked with 100% contain 10 µg (20 µg for analysis of LHCX levels) of protein extracts. Images have been cropped.

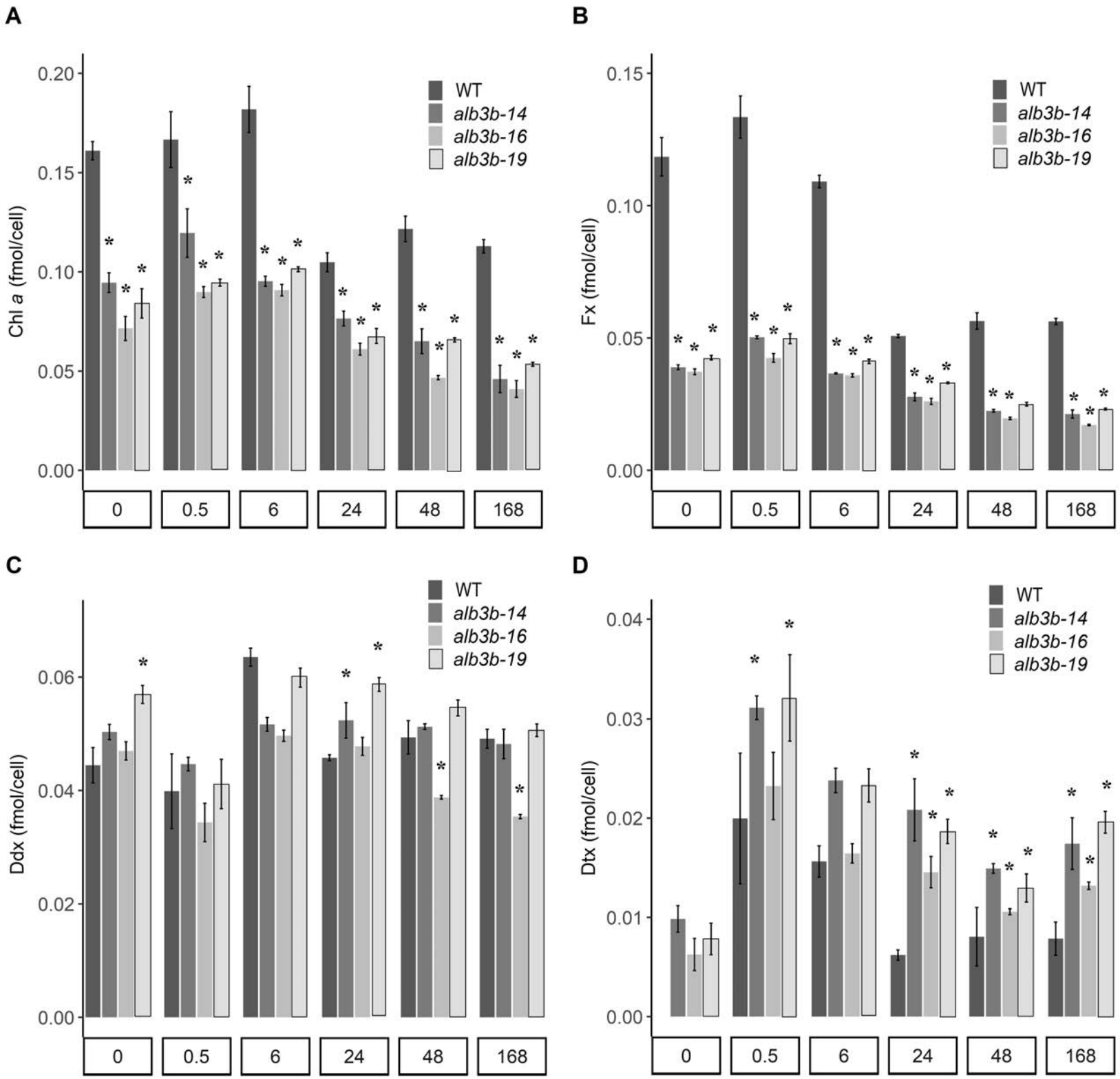

Figure 5 . Pigment concentrations per cell for WT and alb3b mutant lines as a function of ML exposure time. Cellular pigment concentrations of A) Chl *a*, B) Fx, C) Ddx, and D) Dtx in WT and *alb3b* mutant cells as a function of time following a shift from LL conditions (0 h; 35 µmol photons m^{-2} s^{-1}) to ML conditions (200 µmol photons m^{-2} s^{-1}) for 0.5, 6, 24, 48, and 168 h. Results are presented as a mean of three biological replicates with ±SD. Asterisks indicate the results of two-tailed Student *t*-tests: *p<0.05.

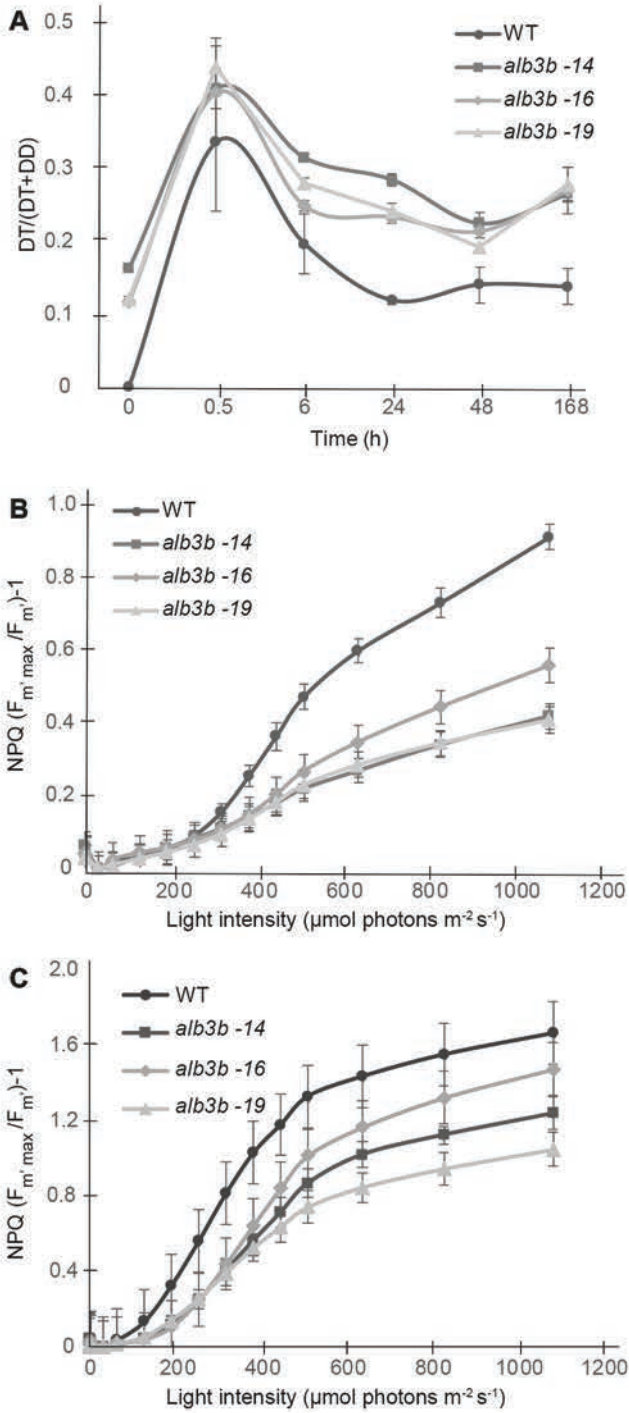

Figure 6. De-epoxidation state index and NPQ capacity of WT and *alb3b* mutants. A) De-epoxidation state index (DES = Dtx/(Dtx + Ddx)) calculated from the HPLC pigment data from LL acclimated (0 h) WT and *alb3b* cultures exposed to ML for 0.5, 6, 24, 48 and 168 h. B) Capacity for NPQ calculated from rapid light curves derived from LL acclimated cells approx. two months after isolation of mutated single cells and C) after being maintained in culture for one more year. NPQ = $(F_{m'max}/F_{m'}) - 1$. $F_{m'max}$ replaces the commonly used F_m since $F_{m'}$ values frequently occur that are higher than the F_m from dark-treated diatom samples (Serôdio et al., 2006). Results are presented as a mean of three biological replicates with ±SD.

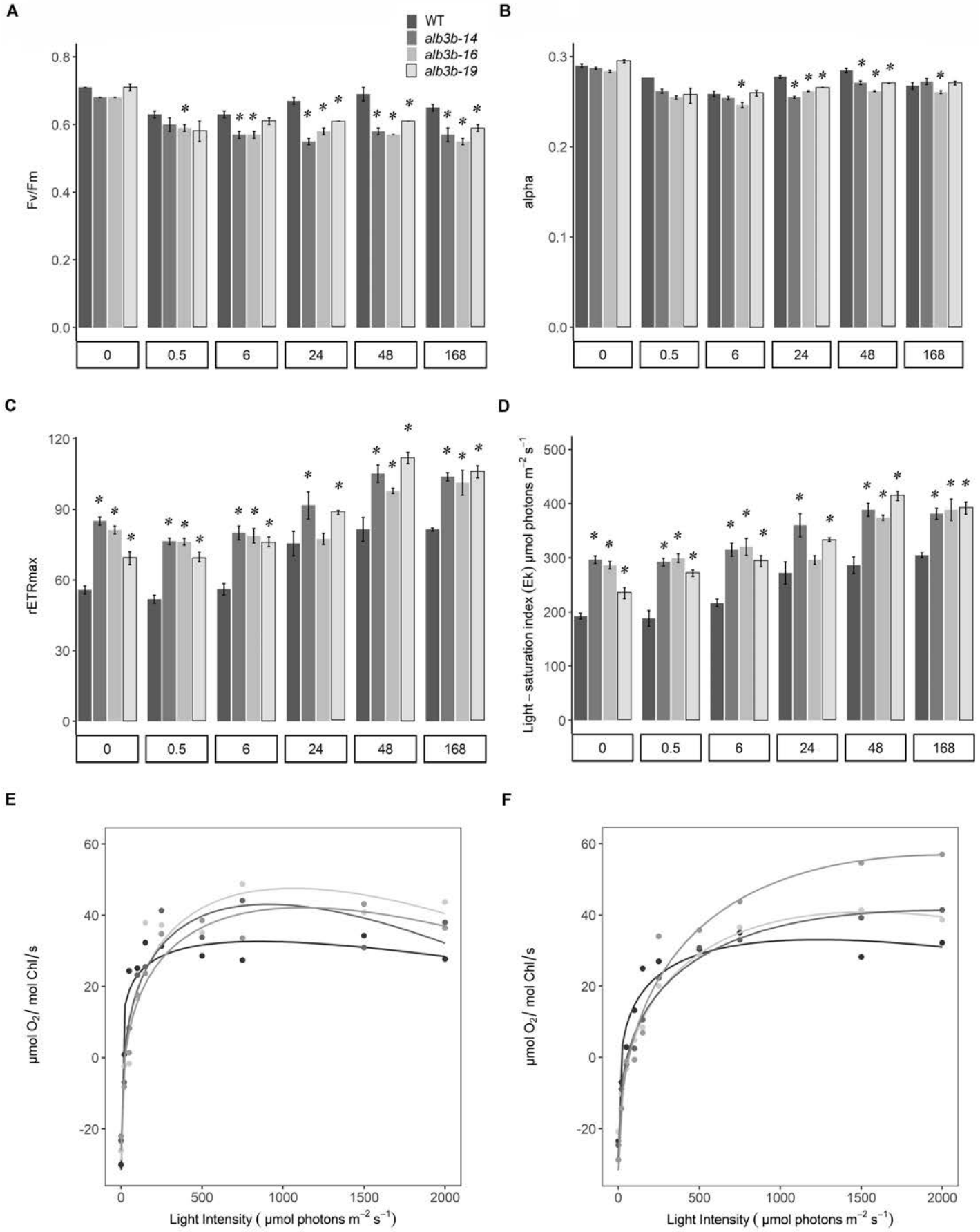

Figure 7 . Photo-physiological responses of WT and *alb3b* mutant lines. In vivo Chl *a* fluorescence kinetics (PAM) were used to estimate A) the maximum quantum yield of PSII (Fv/Fm), B) the maximum light utilization coefficient (α), C) the maximum relative light-saturated electron transport rate (rETRmax), and D) the light saturation index (Ek) in LL (0h) acclimated WT and *alb3b* KO lines as a function of ML exposure time (0.5-168 h). Values are presented with ±SD bars. Asterisks indicate the results of two-tailed Student *t*-tests: *p<0.05. Light-saturation curves of photosynthesis based on oxygen evolution were produced for E) LL- acclimated and F) ML- acclimated WT and alb3b KO lines. The oxygen evolution was normalized on a per-Chl basis. The results were fit with curves based on a polynomial regression using R. All values are presented as an average of three biological replicates for each line and ±SD for each value can be found in Supplementalry Table S3.

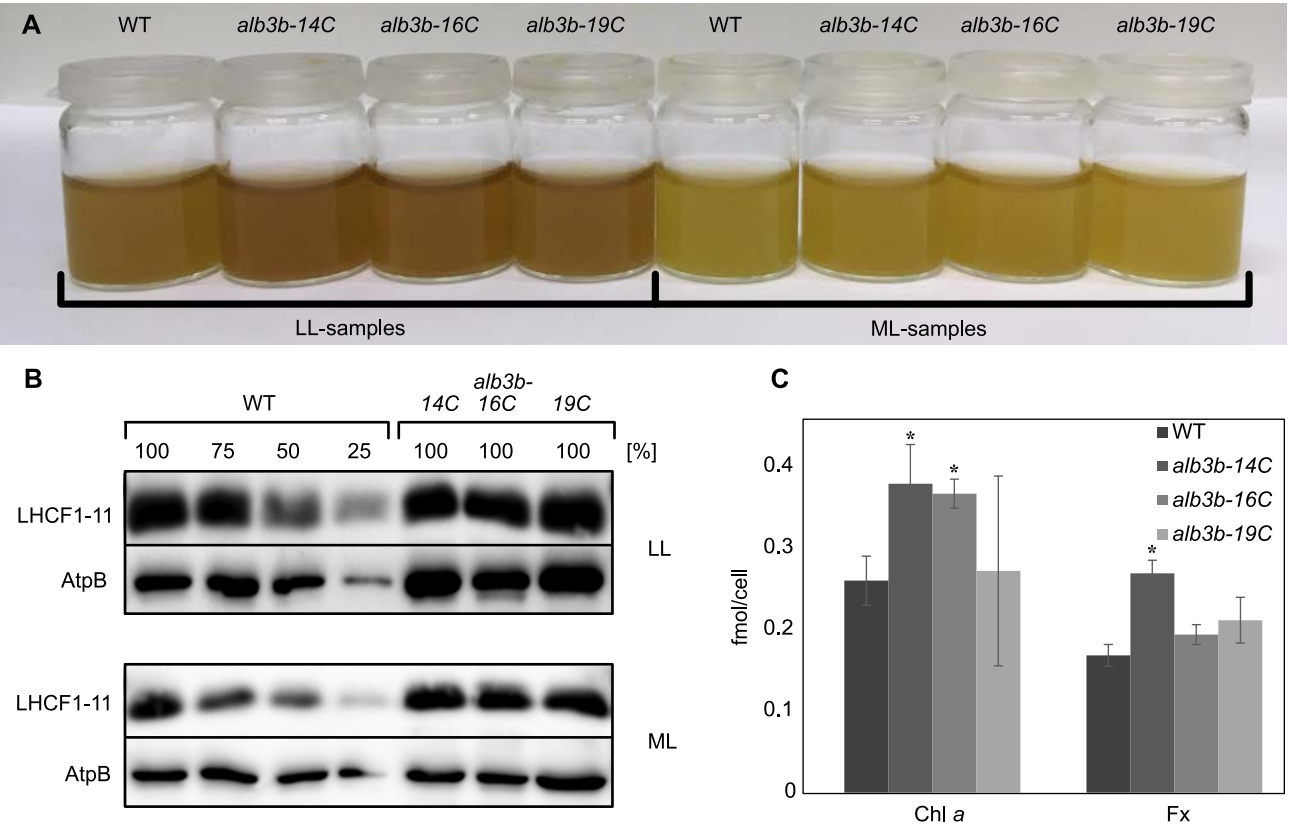

Figure 8. Culture color, LHCF protein level and pigment concentration in complemented *alb3b* lines compared to WT. A) WT and complemented *alb3b* KO lines (*alb3b*-14C, *alb3b*-16C, *alb3b*-19C) were acclimated to LL and ML conditions. All cultures were concentrated and adjusted to equal cell densities (3 x 10^7 cells/ml) for comparison. B) Western blot analysis of LHCF proteins in WT and complemented *alb3b* mutant lines acclimated to LL and ML conditions. LHCF protein levels were evaluated using LHCF1-11 antibody. An antibody recognizing the β-subunit of ATP synthase was used as loading control. 10 µg of total protein from cell lysates was loaded onto the gel. C) Cellular pigment concentrations of Chl *a* and Fx in LL conditions. Results are presented as a mean of three biological replicates with ±SD bars. Asterisks indicate the results of two-tailed Student *t*-tests: *p<0.05.

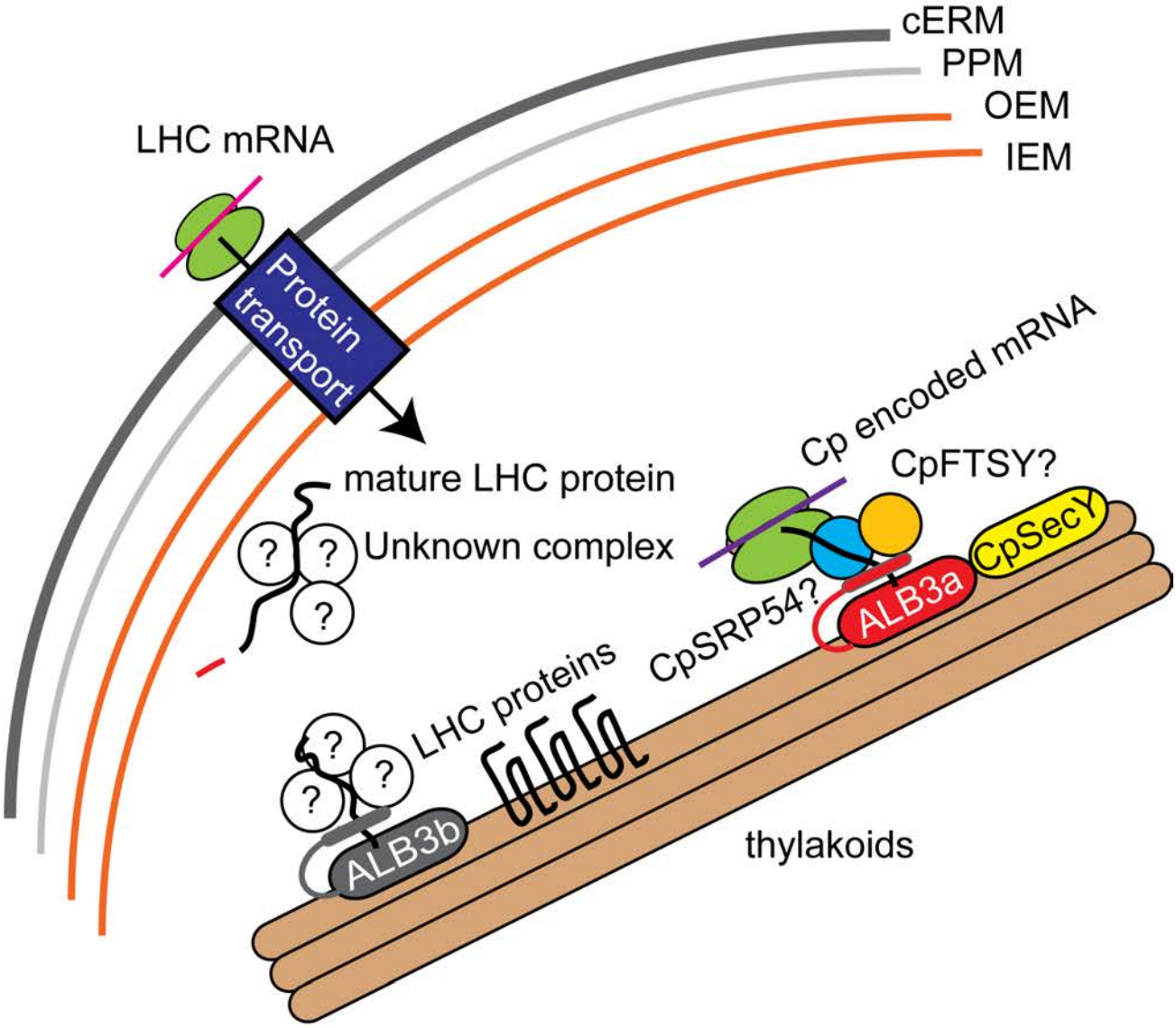

Figure 9. Proposed model of the role of diatom ALB3 insertases in insertion/assembly of thylakoid membrane proteins. LHC proteins are synthesized on ribosomes on the cERM, transported through the four membranes surrounding the secondary plastid of diatoms, and guided to ALB3b by an unknown protein complex before incorporation into the thylakoid membrane (left side). Chloroplast-encoded proteins are suggested to be integrated by the co-translational cpSRP pathway including cpSRP54, FTSY and ALB3ba (right side). cERM: chloroplast ER membrane; PPM: periplastidal membrane; OEM: plastid outer envelope membrane; IEM: plastid inner envelope membrane. CpSRP54: chloroplast signal recognition particle protein 54; CpFTSY: chloroplast SRP receptor; ALB3: chloroplast SRP insertase Albino3.

Parsed Citations

Ago H, Adachi H, Umena Y, Tashiro T, Kawakami K, Kamiya N, Tian L, Han G, Kuang T, Liu Z, Wang F, Zou H, Enami I, Miyano M, Shen JR (2016) Novel features of eukaryotic photosystem II revealed by its crystal structure analysis from a red alga. J Biol Chem 291: 5676-5687

Pubmed: Author and Title
Google Scholar: Author Only Title Only Author and Title

Armbrust EV, Berges JA, Bowler C, Green BR, Martinez D, Putnam NH, Zhou S, Allen AE, Apt KE, Bechner M, Brzezinski MA, Chaal BK, Chiovitti A, Davis AK, Demarest MS, Detter JC, Glavina T, Goodstein D, Hadi MZ, Hellsten U, Hildebrand M, Jenkins BD, Jurka J, Kapitonov VV, Kroger N, Lau WW, Lane TW, Larimer FW, Lippmeier JC, Lucas S, Medina M, Montsant A, Obornik M, Parker MS, Palenik B, Pazour GJ, Richardson PM, Rynearson TA, Saito MA, Schwartz DC, Thamatrakoln K, Valentin K, Vardi A, Wilkerson FP, Rokhsar DS (2004) The genome of the diatom Thalassiosira pseudonana: ecology, evolution, and metabolism. Science 306: 79-86

Pubmed: Author and Title
Google Scholar: Author Only Title Only Author and Title

Austin JR, 2nd, Staehelin LA (2011) Three-dimensional architecture of grana and stroma thylakoids of higher plants as determined by electron tomography. Plant Physiol 155: 1601-1611

Pubmed: Author and Title
Google Scholar: Author Only Title Only Author and Title

Bailleul B, Rogato A, de Martino A, Coesel S, Cardol P, Bowler C, Falciatore A, Finazzi G (2010) An atypical member of the light-harvesting complex stress-related protein family modulates diatom responses to light. Proc Natl Acad Sci U S A 107: 18214-18219

Pubmed: Author and Title
Google Scholar: Author Only Title Only Author and Title

Baroli I, Melis A (1996) Photoinhibition and repair in Dunaliella salina acclimated to different growth irradiances. Planta 198: 640-646

Pubmed: Author and Title
Google Scholar: Author Only Title Only Author and Title

Bellafiore S, Ferris P, Naver H, Gohre V, Rochaix JD (2002) Loss of Albino3 leads to the specific depletion of the light-harvesting system. Plant Cell 14: 2303-2314

Pubmed: Author and Title
Google Scholar: Author Only Title Only Author and Title

Ben-Shem A, Frolow F, Nelson N (2003) Crystal structure of plant photosystem I. Nature 426: 630-635

Pubmed: Author and Title
Google Scholar: Author Only Title Only Author and Title

Bowler C, Allen AE, Badger JH, Grimwood J, Jabbari K, Kuo A, Maheswari U, Martens C, Maumus F, Otillar RP, Rayko E, Salamov A, Vandepoele K, Beszteri B, Gruber A, Heijde M, Katinka M, Mock T, Valentin K, Verret F, Berges JA, Brownlee C, Cadoret JP, Chiovitti A, Choi CJ, Coesel S, De Martino A, Detter JC, Durkin C, Falciatore A, Fournet J, Haruta M, Huysman MJ, Jenkins BD, Jiroutova K, Jorgensen RE, Joubert Y, Kaplan A, Kroger N, Kroth PG, La Roche J, Lindquist E, Lommer M, Martin-Jezequel V, Lopez PJ, Lucas S, Mangogna M, McGinnis K, Medlin LK, Montsant A, Oudot-Le Secq MP, Napoli C, Obornik M, Parker MS, Petit JL, Porcel BM, Poulsen N, Robison M, Rychlewski L, Rynearson TA, Schmutz J, Shapiro H, Siaut M, Stanley M, Sussman MR, Taylor AR, Vardi A, von Dassow P, Vyverman W, Willis A, Wyrwicz LS, Rokhsar DS, Weissenbach J, Armbrust EV, Green BR, Van de Peer Y, Grigoriev IV (2008) The Phaeodactylum genome reveals the evolutionary history of diatom genomes. Nature 456: 239-244

Pubmed: Author and Title
Google Scholar: Author Only Title Only Author and Title

Bozzola JJ, Russell LD (1999) Electron Microscopy: Principles and Techniques for Biologists, Second Edition, Jones and Bartlett, Boston, Publishers.

Bricaud A, Claustre H, Ras J, Oubelkheir K (2004) Natural variability of phytoplanktonic

absorption in oceanic waters: Influence of the size structure of algal populations. J Geophys Res-Oceans 109

Brown JW, Sorhannus U (2010) A molecular genetic timescale for the diversification of autotrophic stramenopiles (Ochrophyta): substantive underestimation of putative fossil ages. PLoS One 5

Pubmed: Author and Title
Google Scholar: Author Only Title Only Author and Title

Büchel C (2014) Fucoxanthin-Chlorophyll-proteins and non-photochemical fluorescence quenching of diatoms. In B Demmig-Adams, G Garab, W Adams III, Govindjee, eds, Non-photochemical quenching and energy dissipation in plants, algae and cyanobacteria. Advances in photosynthesis and respiration (Including bioenergy and related processes), Vol 40. Springer, Dordrecht

Pubmed: Author and Title
Google Scholar: Author Only Title Only Author and Title

Büchel C (2015) Evolution and function of light harvesting proteins. J Plant Physiol 172: 62-75

Pubmed: Author and Title
Google Scholar: Author Only Title Only Author and Title

Chandrasekar S, Shan SO (2017) Anionic phospholipids and the Albino3 translocase activate signal recognition particle-receptor

interaction during light-harvesting chlorophyll a/b-binding protein targeting. J Biol Chem 292: 397-406
Pubmed: Author and Title
Google Scholar: Author Only Title Only Author and Title

Cruz S, Goss R, Wilhelm C, Leegood R, Horton P, Jakob T (2011) Impact of chlororespiration on non-photochemical quenching of chlorophyll fluorescence and on the regulation of the diadinoxanthin cycle in the diatom Thalassiosira pseudonana. J Exp Bot 62: 509-519
Pubmed: Author and Title
Google Scholar: Author Only Title Only Author and Title

Cruz S, Serôdio J (2008) Relationship of rapid light curves of variable fluorescence to photoacclimation and non-photochemical quenching in a benthic diatom. Aquat Bot 88: 256-264
Pubmed: Author and Title
Google Scholar: Author Only Title Only Author and Title

De Martino A, Bartual A, Willis A, Meichenin A, Villazan B, Maheswari U, Bowler C (2011) Physiological and molecular evidence that environmental changes elicit morphological interconversion in the model diatom Phaeodactylum tricornutum. Protist 162: 462-481
Pubmed: Author and Title
Google Scholar: Author Only Title Only Author and Title

De Martino A, Meichenin A, Shi J, Pan KH, Bowler C (2007) Genetic and phenotypic characterization of Phaeodactylum tricornutum (Bacillariophyceae) accessions. J Phycol 43: 992-1009
Pubmed: Author and Title
Google Scholar: Author Only Title Only Author and Title

Durnford DG, Aebersold R, Green BR (1996) The fucoxanthin-chlorophyll proteins from a chromophyte alga are part of a large multigene family: structural and evolutionary relationships to other light harvesting antennae. Mol Gen Genet 253: 377-386
Pubmed: Author and Title
Google Scholar: Author Only Title Only Author and Title

Dünschede B, Bals T, Funke S, Schunemann D (2011) Interaction studies between the chloroplast signal recognition particle subunit cpSRP43 and the full-length translocase Alb3 reveal a membrane-embedded binding region in Alb3 protein. J Biol Chem 286: 35187-35195
Pubmed: Author and Title
Google Scholar: Author Only Title Only Author and Title

Falk S, Ravaud S, Koch J, Sinning I (2010) The C terminus of the Alb3 membrane insertase recruits cpSRP43 to the thylakoid membrane. J Biol Chem 285: 5954-5962
Pubmed: Author and Title
Google Scholar: Author Only Title Only Author and Title

Falk S, Sinning I (2010) The C terminus of Alb3 interacts with the chromodomains 2 and 3 of cpSRP43. J Biol Chem 285: le25-26; author reply le26-28
Pubmed: Author and Title
Google Scholar: Author Only Title Only Author and Title

Falkowski PG, Barber RT, Smetacek V (1998) Biogeochemical controls and feedbacks on ocean primary production. Science 281: 200-206
Pubmed: Author and Title
Google Scholar: Author Only Title Only Author and Title

Falkowski PG, Raven JA (2007) Aquatic photosynthesis, Ed Second edition. Princeton University Press, Princeton
Pubmed: Author and Title
Google Scholar: Author Only Title Only Author and Title

Fawley MW (1984) Effects of llight intensity and temperature interactions on growth characteristics of Phaeodactylum tricornutum (Bacillariophyceae). J Phycol 20: 67-72
Pubmed: Author and Title
Google Scholar: Author Only Title Only Author and Title

Formighieri C, Melis A (2017) Heterologous synthesis of geranyllinalool, a diterpenol plant product, in the cyanobacterium Synechocystis. Appl Microbiol Biotechnol 101: 2791-2800
Pubmed: Author and Title
Google Scholar: Author Only Title Only Author and Title

Genty B, Briantais JM, Baker NR (1989) The relationship between the quantum yield of photosynthetic electron-transport and quenching of chlorophyll fluorescence. Biochim Biophys Acta 990: 87-92
Pubmed: Author and Title
Google Scholar: Author Only Title Only Author and Title

Gerdes L, Bals T, Klostermann E, Karl M, Philippar K, Hunken M, Soll J, Schunemann D (2006) A second thylakoid membrane-localized Alb3/Oxal/YidC homologue is involved in proper chloroplast biogenesis in Arabidopsis thaliana. J Biol Chem 281: 16632-16642
Pubmed: Author and Title
Google Scholar: Author Only Title Only Author and Title

Giovagnetti V, Ruban AV (2017) Detachment of the fucoxanthin chlorophyll a/c binding protein (FCP) antenna is not involved in the acclimative regulation of photoprotection in the pennate diatom Phaeodactylum tricornutum. Biochim Biophys Acta 1858: 218-230
Pubmed: Author and Title
Google Scholar: Author Only Title Only Author and Title

Goss R, Lepetit B (2015) Biodiversity of NPQ. J Plant Physiol 172: 13-32
Pubmed: Author and Title
Google Scholar: Author Only Title Only Author and Title

Grouneva I, Rokka A, Aro EM (2011) The thylakoid membrane proteome of two marine diatoms outlines both diatom-specific and species-specific features of the photosynthetic machinery. J Proteome Res 10: 5338-5353
Pubmed: Author and Title
Google Scholar: Author Only Title Only Author and Title

Gu J, Zhou Z, Li Z, Chen Y, Wang Z, Zhang H, Yang J (2017) Photosynthetic properties and potentials for improvement of photosynthesis in pale green leaf rice under high light conditions. Front Plant Sci 8: 1082
Pubmed: Author and Title
Google Scholar: Author Only Title Only Author and Title

Guenther JE, Melis A (1990) The physiological significance of photosystem II heterogeneity in chloroplasts. Photosynth Res 23: 105-109
Pubmed: Author and Title
Google Scholar: Author Only Title Only Author and Title

Guillard RR, Ryther JH (1962) Studies of marine planktonic diatoms. I. Cyclotella nana Hustedt, and Detonula confervacea (cleve) Gran. Can J Microbiol 8: 229-239
Pubmed: Author and Title
Google Scholar: Author Only Title Only Author and Title

Gundermann K, Büchel C (2014) Structure and functional heterogeneity of fucoxanthin-chlorophyll proteins in diatoms. In M Hohmann-Marriott, ed, The Structural Basis of Biological Energy Generation. Advances in Photosynthesis and Respiration (Including Bioenergy and Related Processes), Vol 39. Springer Dordrecht
Pubmed: Author and Title
Google Scholar: Author Only Title Only Author and Title

Göhre V, Ossenbuhl F, Crevecoeur M, Eichacker LA, Rochaix JD (2006) One of two alb3 proteins is essential for the assembly of the photosystems and for cell survival in Chlamydomonas. Plant Cell 18: 1454-1466
Pubmed: Author and Title
Google Scholar: Author Only Title Only Author and Title

Havaux M, Dall'Osto L, Bassi R (2007) Zeaxanthin has enhanced antioxidant capacity with respect to all other xanthophylls in Arabidopsis leaves and functions independent of binding to PSII antennae. Plant Physiol 145: 1506-1520
Pubmed: Author and Title
Google Scholar: Author Only Title Only Author and Title

Hennon SW, Soman R, Zhu L, Dalbey RE (2015) YidC/Alb3/Oxa1 family of insertases. J Biol Chem 290: 14866-14874
Pubmed: Author and Title
Google Scholar: Author Only Title Only Author and Title

Herbstova M, Bina D, Kana R, Vacha F, Litvin R (2017) Red-light phenotype in a marine diatom involves a specialized oligomeric red-shifted antenna and altered cell morphology. Sci Rep 7: 11976
Pubmed: Author and Title
Google Scholar: Author Only Title Only Author and Title

Hiyama T, Ke B (1972) Difference spectra and extinction coefficients of P700. Biochim Biophys Acta 267: 160-171
Pubmed: Author and Title
Google Scholar: Author Only Title Only Author and Title

Ikeda Y, Komura M, Watanabe M, Minami C, Koike H, Itoh S, Kashino Y, Satoh K (2008) Photosystem I complexes associated with fucoxanthin-chlorophyll-binding proteins from a marine centric diatom, Chaetoceros gracilis. Biochim Biophys Acta 1777: 351-361
Pubmed: Author and Title
Google Scholar: Author Only Title Only Author and Title

Jeffrey SW, Humphrey GF (1975) New spectrophotometric equations for determining chlorophylls a, b, c1 and c2 in higher plants, algae and natural phytoplankton. Biochem Physiol Pfl 167: 191-194
Pubmed: Author and Title
Google Scholar: Author Only Title Only Author and Title

Juhas M, Buchel C (2012) Properties of photosystem I antenna protein complexes of the diatom Cyclotella meneghiniana. J Exp Bot 63: 3673-3681
Pubmed: Author and Title
Google Scholar: Author Only Title Only Author and Title

Juhas M, von Zadow A, Spexard M, Schmidt M, Kottke T, Buchel C (2014) A novel cryptochrome in the diatom Phaeodactylum tricornutum influences the regulation of light-harvesting protein levels. Febs J 281: 2299-2311
Pubmed: Author and Title

Google Scholar: Author Only Title Only Author and Title

Kalaji HM, Schansker G, Brestic M, Bussotti F, Calatayud A, Ferroni L, Goltsev V, Guidi L, Jajoo A, Li P, Losciale P, Mishra VK, Misra AN, Nebauer SG, Pancaldi S, Penella C, Pollastrini M, Suresh K, Tambussi E, Yanniccari M, Zivcak M, Cetner MD, Samborska IA, Stirbet A, Olsovska K, Kunderlikova K, Shelonzek H, Rusinowski S, Baba W (2017) Frequently asked questions about chlorophyll fluorescence, the sequel. Photosynth Res 132: 13-66

Pubmed: Author and Title
Google Scholar: Author Only Title Only Author and Title

Kirst H, Formighieri C, Melis A (2014) Maximizing photosynthetic efficiency and culture productivity in cyanobacteria upon minimizing the phycobilisome light-harvesting antenna size. Bba-Bioenergetics 1837: 1653-1664

Pubmed: Author and Title
Google Scholar: Author Only Title Only Author and Title

Kirst H, Gabilly ST, Niyogi KK, Lemaux PG, Melis A (2017) Photosynthetic antenna engineering to improve crop yields. Planta 245: 1009-1020

Pubmed: Author and Title
Google Scholar: Author Only Title Only Author and Title

Kirst H, Garcia-Cerdan JG, Zurbriggen A, Melis A (2012) Assembly of the light-harvesting chlorophyll antenna in the green alga Chlamydomonas reinhardtii requires expression of the TLA2-CpFTSY gene. Plant Physiol 158: 930-945

Pubmed: Author and Title
Google Scholar: Author Only Title Only Author and Title

Kirst H, Garcia-Cerdan JG, Zurbriggen A, Ruehle T, Melis A (2012) Truncated photosystem chlorophyll antenna size in the green microalga Chlamydomonas reinhardtii upon deletion of the TLA3-CpSRP43 gene. Plant Physiol 160: 2251-2260

Pubmed: Author and Title
Google Scholar: Author Only Title Only Author and Title

Kirst H, Melis A (2014) The chloroplast signal recognition particle (CpSRP) pathway as a tool to minimize chlorophyll antenna size and maximize photosynthetic productivity. Biotechnol Adv 32: 66-72

Pubmed: Author and Title
Google Scholar: Author Only Title Only Author and Title

Kirst H, Shen Y, Vamvaka E, Betterle N, Xu D, Warek U, Strickland JA, Melis A (2018) Downregulation of the CpSRP43 gene expression confers a truncated light-harvesting antenna (TLA) and enhances biomass and leaf-to-stem ratio in Nicotiana tabacum canopies. Planta 248: 139-154

Pubmed: Author and Title
Google Scholar: Author Only Title Only Author and Title

Kugelmann M, Fausser A, Ossenbuhl F, Brennicke A (2013) Phenotypes of Alb3p and carotenoid synthesis mutants show similarities regarding light sensitivity, thylakoid structure and protein stability. Photosynthetica 51: 45-54

Pubmed: Author and Title
Google Scholar: Author Only Title Only Author and Title

Kumar S, Stecher G, Tamura K (2016) MEGA7: Molecular Evolutionary Genetics Analysis Version 7.0 for Bigger Datasets. Mol Biol Evol 33: 1870-1874

Pubmed: Author and Title
Google Scholar: Author Only Title Only Author and Title

Lamb J, Forfang K, Hohmann-Marriott M (2015) A practical solution for 77 K fluorescence measurements based on LED excitation and CCD array detector. PLoS One 10: e0132258

Pubmed: Author and Title
Google Scholar: Author Only Title Only Author and Title

Lang M, Kroth PG (2001) Diatom fucoxanthin chlorophyll a/c-binding protein (FCP) and land plant light-harvesting proteins use a similar pathway for thylakoid membrane Insertion. J Biol Chem 276: 7985-7991

Pubmed: Author and Title
Google Scholar: Author Only Title Only Author and Title

Lavaud J, Goss R (2014) The peculiar features of non-photochemical fluorescence quenching in diatoms and brown algae. In B Demmig-Adams, G Garab, IW Adams, Govindjee, eds, Non-photochemical quenching and energy dissipation in plants, algae and cyanobacteria. Advances in photosynthesis and respiration (Including bioenergy and related processes), Vol 40. Springer, Dordrecht

Pubmed: Author and Title
Google Scholar: Author Only Title Only Author and Title

Lavaud J, Lepetit B (2013) An explanation for the inter-species variability of the photoprotective non-photochemical chlorophyll fluorescence quenching in diatoms. Biochim Biophys Acta 1827: 294-302

Pubmed: Author and Title
Google Scholar: Author Only Title Only Author and Title

Lavaud J, Rousseau B, van Gorkom HJ, Etienne AL (2002) Influence of the diadinoxanthin pool size on photoprotection in the marine planktonic diatom Phaeodactylum tricornutum. Plant Physiol 129: 1398-1406

Pubmed: Author and Title
Google Scholar: Author Only Title Only Author and Title

Le SQ, Gascuel O (2008) An improved general amino acid replacement matrix. Mol Biol Evol 25: 1307-1320
Pubmed: Author and Title
Google Scholar: Author Only Title Only Author and Title

Lepetit B, Gelin G, Lepetit M, Sturm S, Vugrinec S, Rogato A, Kroth PG, Falciatore A, Lavaud J (2017) The diatom Phaeodactylum tricornutum adjusts nonphotochemical fluorescence quenching capacity in response to dynamic light via fine-tuned Lhcx and xanthophyll cycle pigment synthesis. New Phytol 214: 205-218
Pubmed: Author and Title
Google Scholar: Author Only Title Only Author and Title

Lepetit B, Goss R, Jakob T, Wilhelm C (2012) Molecular dynamics of the diatom thylakoid membrane under different light conditions. Photosynth Res 111: 245-257
Pubmed: Author and Title
Google Scholar: Author Only Title Only Author and Title

Lepetit B, Sturm S, Rogato A, Gruber A, Sachse M, Falciatore A, Kroth PG, Lavaud J (2013) High light acclimation in the secondary plastids containing diatom Phaeodactylum tricornutum is triggered by the redox state of the plastoquinone pool. Plant Physiol 161: 853-865
Pubmed: Author and Title
Google Scholar: Author Only Title Only Author and Title

Lepetit B, Volke D, Gilbert M, Wilhelm C, Goss R (2010) Evidence for the existence of one antenna-associated, lipid-dissolved and two protein-bound pools of diadinoxanthin cycle pigments in diatoms. Plant Physiol 154: 1905-1920
Pubmed: Author and Title
Google Scholar: Author Only Title Only Author and Title

Lewis NE, Marty NJ, Kathir KM, Rajalingam D, Kight AD, Daily A, Kumar TK, Henry RL, Goforth RL (2010) A dynamic cpSRP43-Albino3 interaction mediates translocase regulation of chloroplast signal recognition particle (cpSRP)-targeting components. J Biol Chem 285: 34220-34230
Pubmed: Author and Title
Google Scholar: Author Only Title Only Author and Title

Madhuri S, Serif M, Rio Bartulos C, Lepetit B, Kroth PG (2019) A strategy to complement PtAUREO1a in TALEN knockout strains of Phaeodactylum tricornutum. Algal Res 39: 101469
Pubmed: Author and Title
Google Scholar: Author Only Title Only Author and Title

Melis A (1989) Spectroscopic methods in photosynthesis - Photosystem stoichiometry and chlorophyll antenna size. Philos T Roy Soc B 323: 397-409
Pubmed: Author and Title
Google Scholar: Author Only Title Only Author and Title

Melis A, Brown JS (1980) Stoichiometry of system I and system II reaction centers and of plastoquinone in different photosynthetic membranes. P Natl Acad Sci-Biol 77: 4712-4716
Pubmed: Author and Title
Google Scholar: Author Only Title Only Author and Title

Miloslavina Y, Grouneva I, Lambrev PH, Lepetit B, Goss R, Wilhelm C, Holzwarth AR (2009) Ultrafast fluorescence study on the location and mechanism of non-photochemical quenching in diatoms. Biochim Biophys Acta 1787: 1189-1197
Pubmed: Author and Title
Google Scholar: Author Only Title Only Author and Title

Mock T, Otillar RP, Strauss J, McMullan M, Paajanen P, Schmutz J, Salamov A, Sanges R, Toseland A, Ward BJ, Allen AE, Dupont CL, Frickenhaus S, Maumus F, Veluchamy A, Wu T, Barry KW, Falciatore A, Ferrante MI, Fortunato AE, Glöckner G, Gruber A, Hipkin R, Janech MG, Kroth PG, Leese F, Lindquist EA, Lyon BR, Martin J, Mayer C, Parker M, Quesneville H, Raymond JA, Uhlig C, Valas RE, Valentin KU, Worden AZ, Armbrust EV, Clark MD, Bowler C, Green BR, Moulton V, van Oosterhout C, Grigoriev IV (2017) Evolutionary genomics of the cold-adapted diatom Fragilariopsis cylindrus. Nature 541: 536
Pubmed: Author and Title
Google Scholar: Author Only Title Only Author and Title

Moore M, Harrison MS, Peterson EC, Henry R (2000) Chloroplast Oxa1p homolog albino3 is required for post-translational integration of the light harvesting chlorophyll-binding protein into thylakoid membranes. J Biol Chem 275: 1529-1532
Pubmed: Author and Title
Google Scholar: Author Only Title Only Author and Title

Nelson N, Yocum CF (2006) Structure and function of photosystems I and II. Annu Rev Plant Biol 57: 521-565
Pubmed: Author and Title
Google Scholar: Author Only Title Only Author and Title

Nicholas KB, Nicholas HBJ, Deerfield DWI (1997) GeneDoc: analysis and visualization of genetic variation. EMBNEW. NEWS 4
Pubmed: Author and Title
Google Scholar: Author Only Title Only Author and Title

Nymark M, Sharma AK, Hafskjold MC, Sparstad T, Bones AM, Winge P (2017) CRISPR/Cas9 Gene editing in the marine diatom Phaeodactylum tricornutum. Bio-protocol 7: e2442
Pubmed: Author and Title
Google Scholar: Author Only Title Only Author and Title

Nymark M, Sharma AK, Sparstad T, Bones AM, Winge P (2016) A CRISPR/Cas9 system adapted for gene editing in marine algae. Sci Rep-Uk 6
Pubmed: Author and Title
Google Scholar: Author Only Title Only Author and Title

Nymark M, Valle KC, Brembu T, Hancke K, Winge P, Andresen K, Johnsen G, Bones AM (2009) An integrated analysis of molecular acclimation to high light in the marine diatom Phaeodactylum tricornutum. PLoS ONE 4: e7743
Pubmed: Author and Title
Google Scholar: Author Only Title Only Author and Title

Nymark M, Valle KC, Hancke K, Winge P, Andresen K, Johnsen G, Bones AM, Brembu T (2013) Molecular and photosynthetic responses to prolonged darkness and subsequent acclimation to re-illumination in the diatom Phaeodactylum tricornutum. PLoS ONE 8: e58722
Pubmed: Author and Title
Google Scholar: Author Only Title Only Author and Title

Oey M, Ross IL, Stephens E, Steinbeck J, Wolf J, Radzun KA, Kugler J, Ringsmuth AK, Kruse O, Hankamer B (2013) RNAi knock-down of LHCBM1, 2 and 3 Increases photosynthetic H2 production efficiency of the green alga Chlamydomonas reinhardtii. Plos One 8
Pubmed: Author and Title
Google Scholar: Author Only Title Only Author and Title

Ossenbühl F, Gohre V, Meurer J, Krieger-Liszkay A, Rochaix JD, Eichacker LA (2004) Efficient assembly of photosystem II in Chlamydomonas reinhardtii requires Alb3.1p, a homolog of Arabidopsis ALBINO3. Plant Cell 16: 1790-1800
Pubmed: Author and Title
Google Scholar: Author Only Title Only Author and Title

Oudot-Le Secq MP, Grimwood J, Shapiro H, Armbrust EV, Bowler C, Green BR (2007) Chloroplast genomes of the diatoms Phaeodactylum tricornutum and Thalassiosira pseudonana: comparison with other plastid genomes of the red lineage. Mol Genet Genomics 277: 427-439
Pubmed: Author and Title
Google Scholar: Author Only Title Only Author and Title

Polle JE, Kanakagiri SD, Melis A (2003) Tla1, a DNA insertional transformant of the green alga Chlamydomonas reinhardtii with a truncated light-harvesting chlorophyll antenna size. Planta 217: 49-59
Pubmed: Author and Title
Google Scholar: Author Only Title Only Author and Title

Powles SB, Critchley C (1980) Effect of light intensity during growth on photoinhibition of intact attached bean leaflets. Plant Physiol 65: 1181-1187
Pubmed: Author and Title
Google Scholar: Author Only Title Only Author and Title

Premvardhan L, Bordes L, Beer A, Büchel C, Robert B (2009) Carotenoid structures and environments in trimeric and oligomeric fucoxanthin chlorophyll a/c2 proteins from resonance Raman spectroscopy. J Phys Chem B 113: 12565-12574
Pubmed: Author and Title
Google Scholar: Author Only Title Only Author and Title

Premvardhan L, Robert B, Beer A, Büchel C (2010) Pigment organization in fucoxanthin chlorophyll a/c2 proteins (FCP) based on resonance Raman spectroscopy and sequence analysis. Biochim Biophys Acta 1797: 1647-1656
Pubmed: Author and Title
Google Scholar: Author Only Title Only Author and Title

Ramakers C, Ruijter JM, Deprez RH, Moorman AF (2003) Assumption-free analysis of quantitative real-time polymerase chain reaction (PCR) data. Neurosci Lett 339: 62-66
Pubmed: Author and Title
Google Scholar: Author Only Title Only Author and Title

Rodriguez F, Chauton M, Johnsen G, Andresen K, Olsen LM, Zapata M (2006) Photoacclimation in phytoplankton: implications for biomass estimates, pigment functionality and chemotaxonomy. Mar Biol 148: 963-971
Pubmed: Author and Title
Google Scholar: Author Only Title Only Author and Title

Ruijter JM, Ramakers C, Hoogaars WM, Karlen Y, Bakker O, van den Hoff MJ, Moorman AF (2009) Amplification efficiency: linking baseline and bias in the analysis of quantitative PCR data. Nucleic Acids Res 37: e45
Pubmed: Author and Title
Google Scholar: Author Only Title Only Author and Title

Saitou N, Nei M (1987) The neighbor-joining method: a new method for reconstructing phylogenetic trees. Mol Biol Evol 4: 406-425
Pubmed: Author and Title
Google Scholar: Author Only Title Only Author and Title

Sakshaug E, Bricaud A, Dandonneau Y, Falkowski PG, Kiefer DA, Legendre L, Morel A, Parslow J, Takahashi M (1997) Parameters of photosynthesis: definitions, theory and interpretation of results. J Plankton Res 19: 1637-1670
Pubmed: Author and Title
Google Scholar: Author Only Title Only Author and Title

Schuenemann D, Gupta S, Persello-Cartieaux F, Klimyuk VI, Jones JD, Nussaume L, Hoffman NE (1998) A novel signal recognition particle targets light-harvesting proteins to the thylakoid membranes. Proc Natl Acad Sci U S A 95: 10312-10316
Pubmed: Author and Title
Google Scholar: Author Only Title Only Author and Title

Serif M, Lepetit B, Weißert K, Kroth PG, Rio Bartulos C (2017) A fast and reliable strategy to generate TALEN-mediated gene knockouts in the diatom Phaeodactylum tricornutum. Algal Res 23: 186-195
Pubmed: Author and Title
Google Scholar: Author Only Title Only Author and Title

Serôdio J, Vieira S, Cruz S, Coelho H (2006) Rapid light-response curves of chlorophyll fluorescence in microalgae: relationship to steady-state light curves and non-photochemical quenching in benthic diatom-dominated assemblages. Photosynth Res 90: 29-43
Pubmed: Author and Title
Google Scholar: Author Only Title Only Author and Title

Sundberg E, Slagter JG, Fridborg I, Cleary SP, Robinson C, Coupland G (1997) ALBINO3, an Arabidopsis nuclear gene essential for chloroplast differentiation, encodes a chloroplast protein that shows homology to proteins present in bacterial membranes and yeast mitochondria. Plant Cell 9: 717-730
Pubmed: Author and Title
Google Scholar: Author Only Title Only Author and Title

Taddei L, Chukhutsina VU, Lepetit B, Stella GR, Bassi R, van Amerongen H, Bouly JP, Jaubert M, Finazzi G, Falciatore A (2018) Dynamic changes between two LHCX-related energy quenching sites control diatom photoacclimation. Plant Physiol 177: 953-965
Pubmed: Author and Title
Google Scholar: Author Only Title Only Author and Title

Taddei L, Stella GR, Rogato A, Bailleul B, Fortunato AE, Annunziata R, Sanges R, Thaler M, Lepetit B, Lavaud J, Jaubert M, Finazzi G, Bouly JP, Falciatore A (2016) Multisignal control of expression of the LHCX protein family in the marine diatom Phaeodactylum tricornutum. J Exp Bot 67: 3939-3951
Pubmed: Author and Title
Google Scholar: Author Only Title Only Author and Title

Theis J, Schroda M (2016) Revisiting the photosystem II repair cycle. Plant Signal Behav 11: e1218587
Pubmed: Author and Title
Google Scholar: Author Only Title Only Author and Title

Thompson JD, Gibson TJ, Plewniak F, Jeanmougin F, Higgins DG (1997) The CLUSTAL_X windows interface: flexible strategies for multiple sequence alignment aided by quality analysis tools. Nucleic Acids Res 25: 4876-4882
Pubmed: Author and Title
Google Scholar: Author Only Title Only Author and Title

Träger C, Rosenblad MA, Ziehe D, Garcia-Petit C, Schrader L, Kock K, Richter CV, Klinkert B, Narberhaus F, Herrmann C, Hofmann E, Aronsson H, Schunemann D (2012) Evolution from the prokaryotic to the higher plant chloroplast signal recognition particle: the signal recognition particle RNA is conserved in plastids of a wide range of photosynthetic organisms. Plant Cell 24: 4819-4836
Pubmed: Author and Title
Google Scholar: Author Only Title Only Author and Title

Valle KC, Nymark M, Aamot I, Hancke K, Winge P, Andresen K, Johnsen G, Brembu T,

Bones AM (2014) System responses to equal doses of photosynthetically usable radiation of blue, green, and red light in the marine diatom Phaeodactylum tricornutum. PLoS One 9: e114211
Pubmed: Author and Title
Google Scholar: Author Only Title Only Author and Title

Yamagishi A, Ikeda Y, Komura M, Koike H, Satoh K, Itoh S, Shibata Y (2010) Shallow sink in

an antenna pigment system of photosystem I of a marine centric diatom, Chaetoceros gracilis, revealed by ultrafast fluorescence spectroscopy at 17 K. J Phys Chem B 114: 9031-9038
Pubmed: Author and Title
Google Scholar: Author Only Title Only Author and Title

Wang W, Yu L-J, Xu C, Tomizaki T, Zhao S, Umena Y, Chen X, Qin X, Xin Y, Suga M, Han

G, Kuang T, Shen J-R (2019) Structural basis for blue-green light harvesting and energy dissipation in diatoms. Science 363: eaav0365
Pubmed: Author and Title
Google Scholar: Author Only Title Only Author and Title